

The role of mitochondrial dynamics and
metabolism in neuroblast differentiation in
Drosophila melanogaster

A Thesis

submitted to
Indian Institute of Science Education and Research, Pune
in partial fulfillment of the requirements for the
BS-MS Dual Degree Programme by

Prachiti Moghe

20131123



Indian Institute of Science Education and Research Pune
Dr. Homi Bhabha Road,
Pashan, Pune 411008, INDIA.

March 2018

Supervisor: Dr. Richa Rikhy, Division of Biology, IISER Pune
TAC Member: Dr. Anuradha Ratnaparkhi, Agharkar Research Institute, Pune

©Prachiti Moghe 2018
All rights reserved

Certificate

This is to certify that this dissertation entitled “***The role of mitochondrial dynamics and metabolism in neuroblast differentiation in Drosophila melanogaster***” towards the partial fulfilment of the BS-MS dual degree programme at the Indian Institute of Science Education and Research (IISER), Pune represents study/work carried out by **Prachiti Moghe** at the Indian Institute of Science Education and Research, Pune under the supervision of **Dr. Richa Rikhy, Associate Professor, Division of Biology, IISER Pune** during the academic year 2017-18.



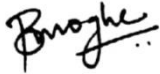
Prachiti Moghe
5th Year BS-MS
20131123



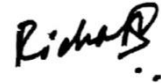
Dr. Richa Rikhy
Associate Professor
Division of Biology, IISER Pune

Declaration

I hereby declare that the matter embodied in the report entitled “***The role of mitochondrial dynamics and metabolism in neuroblast differentiation in Drosophila melanogaster***” are the results of the work carried out by me at the Division of Biology, Indian Institute of Science Education and Research, Pune, under the supervision of **Dr. Richa Rikhy** and the same has not been submitted elsewhere for any other degree.



Prachiti Moghe
5th Year BS-MS
20131123



Dr. Richa Rikhy
Associate Professor
Division of Biology, IISER Pune

Acknowledgments

The project was only possible due to the guidance provided by Dr. Richa Rikhy, my thesis advisor. I am immensely grateful for her support throughout the project. It has been an incredible experience working in the Morphogenesis and Differentiation 'MAD' lab. I would like to thank Dnyanesh Dubal for being so helpful during the entire course of this project, ever since I joined the lab as a semester project student. My sincerest thanks to Gayatri, who has been by my side throughout the final year at IISER; from troubleshooting STED to sorting pupae at absurd hours, we have been through it all! I would like to thank Darshika and Sayali for persistently answering the most fundamental questions I had related to mitochondria; and Bhavin, Sameer, Bipasha, and Swati for offering input and suggestions, and always being entertaining and fun. The atmosphere in the lab has been very positive and stimulating.

I would like to thank Dr. Anuradha Ratnaparkhi for feedback during the project and being my TAC member. I appreciate Dr. Girish Ratnaparkhi and GR Lab members for discussions and input during lab meetings. I also want to thank the IISER Pune Fly Facility and Microscopy Facility and those associated with it for infrastructure and making experimental work smoother. I want to thank the INSPIRE Fellowship for funding during the BS-MS course and means to attend multiple conferences and meetings.

Thank you to my friends in IISER- Nabha, Ira, Divya, and Mekhala for making these five years so memorable. To my friends of 19 years- Namita, Aishwarya, Annushka, Anoushka, and Sayali, thank you for being constant sources of joy and inspiration! Lastly, my deepest thanks to my amazing family - my parents, Pradeep and Pratibha, and my sister Pranoti, for being the best support system one could have.

It always seems impossible until it's done.

Contents

Abstract	1
List of Figures	2
List of Tables	2
1. Introduction	3
1.1. Regulation of mitochondrial morphology	3
1.2. Mitochondrial metabolism	4
1.3. Interaction between mitochondria and signaling pathways	5
1.4. <i>Drosophila</i> neuroblasts as a model to study mitochondrial functions during cell differentiation	6
1.5. Notch signaling in <i>Drosophila</i> NBs	7
1.6. Objectives	8
2. Materials and Methods	10
2.1 <i>Drosophila</i> stocks and crosses	10
2.2 Immunostaining	10
2.3 Manipulation of cellular functions using pharmacological treatment	11
2.4 Microscopy	12
2.5 Image analysis for cell counting and fluorescence estimation	13
3. Results	15
3.1 Depletion of Marf and Opa1 decreases mitochondrial fusion and depletion of Drp1 increases mitochondrial fusion in <i>Drosophila</i> type-II neuroblasts	15
3.2 Inhibition of mitochondrial fusion in <i>marf</i> and <i>opa1</i> results in a decrease in the number of differentiated cells in the type-II neuroblast lineage	16
3.3 Forced mitochondrial fusion by inhibition of <i>drp1</i> -mediated fission in <i>marf</i> and <i>opa1</i> background rescues the loss of differentiated cells in the type-II neuroblast lineage	18
3.4 Cellular effects of inhibition of mitochondrial fusion in <i>marf</i> and <i>opa1</i>	20
3.4.1 Analysis of cell cycle, apoptosis and DNA damage on depletion of <i>marf</i> and <i>opa1</i> in type-II neuroblasts	20
3.4.2 Analysis of mitochondrial activity in the form of pAMPK, cytochrome-c and ROS levels on depletion of <i>marf</i> and <i>opa1</i> in type-II neuroblasts	22
3.4.3 Notch signaling is abrogated in type-II neuroblasts depleted of Marf and Opa1	24
3.5 Notch signaling maintains fused mitochondria in the type-II neuroblasts	25
3.6 Analysis of inhibition of the mitochondrial electron transport chain on mitochondrial morphology and differentiation of type-II NBs	31
3.6.1 Depletion of ETC ComplexIV decreases the number of differentiated cells in the type-II neuroblast lineage	31
3.6.2 Mitochondrial morphology is fragmented on pharmacological ETC disruption, but this does not affect NICD distribution	34
4. Discussion	36
5. References	41
6. Appendix	44

Abstract

Mitochondria regulate various cellular processes such as the production of ATP, generation of ROS, calcium buffering and apoptosis. The mitochondrial network is actively remodeled through cycles of fusion and fission, and mitochondrial defects are associated with diseases. It is clear that mitochondrial functions in differentiated tissues are highly regulated; however, their role in cell differentiation is not extensively studied. We focussed on *Drosophila* neural stem cells, called neuroblasts, to analyze mitochondrial functions during cell differentiation using a genetics approach. We examined the differentiation of type-II neuroblasts after perturbing mitochondrial dynamics and metabolism by targeting mitochondrial fusion proteins Opa1 and Marf, fission protein Drp1, and Complex-IV of the electron transport chain, allowing for the elucidation of the role of mitochondrial functions in neuroblast differentiation. Tissue-specific depletion of Opa1 reduced mitochondrial fusion in neuroblasts with a concomitant decrease in the number of differentiated progeny produced by the neuroblasts. Additionally, inhibition of mitochondrial fusion resulted in reduced Notch signaling, increased cytochrome-c and reactive oxygen species in the type-II neuroblasts. In comparison, we observed hyper-fused mitochondria in Drp1 mutants, which surprisingly had no effect on neuroblast differentiation. Further, suppression of the activity of the electron transport chain by depletion of mitochondrial Complex-IV also decreased neuroblast differentiation. We thus hypothesize that fused mitochondria are a prerequisite in neuroblasts for sustaining proper signaling activity. Our studies have also revealed cross-talk between Notch signaling and mitochondrial dynamics - Notch signaling maintains fused mitochondria in type-II neuroblasts possibly by regulating the expression of mitochondrial fusion genes; and fragmented mitochondria hinder Notch signaling, subsequently inhibiting the production of differentiated cells.

List of figures

No.	Title	Page No.
Introduction		
1.1	Schematic representation of mitochondrial fusion and fission	3
1.2	Schematic representation of the mitochondrial electron transport chain	4
1.3	Asymmetric cell division and lineage progression of <i>Drosophila</i> neuroblasts	7
1.4	Summary of the canonical Notch signaling pathway	8
Results		
3.1	Depletion of Marf and Opa1 decreases mitochondrial fusion and depletion of Drp1 increases mitochondrial fusion in <i>Drosophila</i> type-II neuroblasts	15
3.2	Inhibition of mitochondrial fusion in <i>marf</i> and <i>opa1</i> results in a decrease in the number of differentiated cells in the type-II neuroblast lineage	17
3.3	Forced mitochondrial fusion by inhibition of <i>drp1</i> -mediated fission in <i>marf</i> and <i>opa1</i> background rescues the loss of differentiated cells in the type-II neuroblast lineage	19
3.4.1	Cellular effects of inhibition of mitochondrial fusion in <i>marf</i> and <i>opa1</i>	21
3.4.2	Inhibition of mitochondrial fusion in <i>marf</i> and <i>opa1</i> increases cytochrome-c and ROS in the type-II NBs	23
3.4.3	Inhibition of mitochondrial fusion in <i>marf</i> and <i>opa1</i> causes cytoplasmic accumulation of cleaved NICD in type-II NBs	25
3.5.1	Depletion of Marf and Opa1 alleviates Notch-mediated type-II NB hyperproliferation	26
3.5.2	Notch signaling maintains a fused mitochondrial morphology in type-II neuroblasts	27
3.5.3	Notch signaling maintains fused mitochondria in type-II neuroblasts	29
3.5.4	Fused mitochondria allow production of differentiated cells on downregulation of Notch signaling	30
3.6.1	Inhibition of ETC in type-II neuroblasts causes differentiation defects in <i>cova</i> mutants	32
3.6.2	Inhibition of ETC in type-II neuroblasts decreases ROS and does not affect cytochrome-c in <i>cova</i> mutants	33,34
3.6.3	Analysis of mitochondrial morphology upon inhibition of the ETC	35
Discussion		
4.1	Schematic model of the role played by mitochondrial morphology in the differentiation of type-II neuroblasts	37

List of tables

Materials and Methods

2.1	List of antibodies and dyes used in the project	11
-----	---	----

1. Introduction

1.1. Regulation of mitochondrial morphology

Mitochondria are famously known for adenosine 5'-triphosphate (ATP) generation and metabolism of carbohydrates, lipids, and proteins (Mcbride and Neuspiel, 2006). The activity of the electron transport chain gives rise to reactive oxygen species as a by-product during ATP synthesis. Mitochondria also buffer calcium in the cell and play a significant role in apoptosis. Moreover, they are highly dynamic organelles that change their morphology through fission and fusion events. Mitochondrial dynamics and morphology are regulated by dynamin-superfamily GTPase proteins (Chan, 2006) – mitofusins 1 and 2 (MFN1 and MFN2) anchored on the mitochondria facilitate fusion of the outer membrane by forming dimers, and optic atrophy 1 (OPA1) mediates fusion of the inner membrane and maintains cristae structure (Fig.1.1). Fusion allows homogenization of mitochondrial proteins, enhancement of the respiratory complexes, and complementation of mitochondrial DNA (Mishra and Chan, 2014). Likewise, fission of mitochondria contributes to their quality control and leads to mitophagy of damaged mitochondria. Dynamin-related protein 1 (DRP1) and Fission 1 (FIS1) govern fission along with other receptors for DRP1 on the mitochondrial outer membrane such as mitochondrial fission factor (MFF), MiD49 and MiD51. In *Drosophila*, mitochondrial dynamics is regulated by the fusion proteins *opa1-like* (Opa1, a homolog of OPA1), and mitochondrial assembly regulatory factor (Marf, a homolog of MFN2), and fission proteins Drp1 and Fis1.

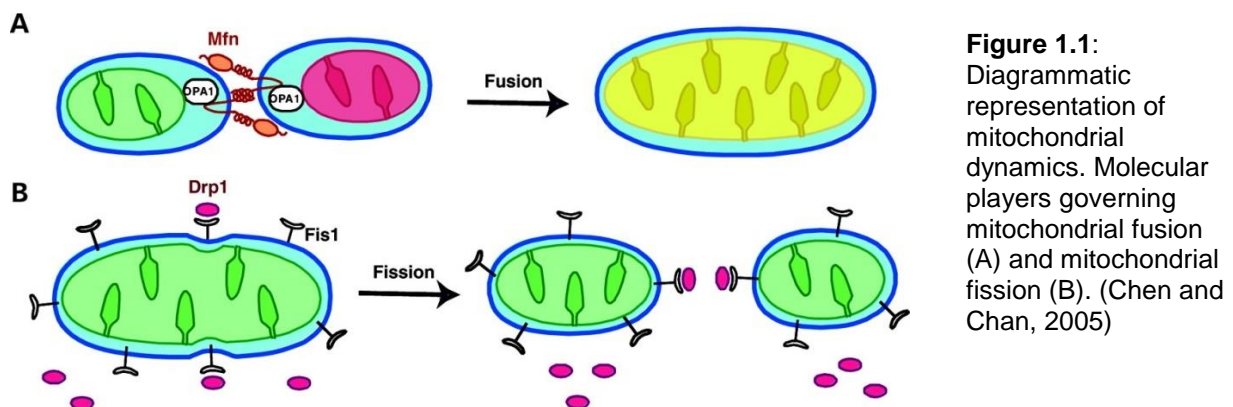


Figure 1.1: Diagrammatic representation of mitochondrial dynamics. Molecular players governing mitochondrial fusion (A) and mitochondrial fission (B). (Chen and Chan, 2005)

Defects in mitochondrial dynamics, energetics, transport or mitophagy in cells of the nervous system are known to cause neurodegenerative diseases (Chen and Chan, 2009). Mutations in fusion protein MFN2 cause Charcot–Marie–Tooth neuropathy type 2A in humans, a disease affecting motor and sensory neurons in the peripheral nervous system (Züchner et al., 2004). Likewise, mutations in OPA1 cause dominant

optic atrophy characterized by progressive degeneration of the optic nerve and loss of vision (Alexander et al., 2000). Apart from its role in mitochondrial fusion, Opa1 is also regulates inner membrane cristae junctions in mitochondria (Frezza et al., 2006) by keeping the cristae pockets ‘tight’ to prevent the release of cytochrome-c. Therefore, it is clear that mitochondrial function in differentiated tissues is a highly regulated process. In contrast, the role of mitochondrial morphology and metabolism during stem cell differentiation remains relatively less explored.

1.2. Mitochondrial metabolism

During cellular metabolism, glycolysis breaks down carbohydrates such as glucose to pyruvate, which enters the mitochondria (Wallace et al., 2011) and is converted into acetyl-CoA. Acetyl-CoA is incorporated into the tricarboxylic acid cycle (TCA) in the mitochondrial matrix, whose outputs are electron carriers that feed into the electron transport chain (ETC) in the inner mitochondrial membrane. The electron transport chain comprises five major protein complexes I, II, III, IV, and V embedded in the cristae folds (Fig.1.2) and is responsible for ATP production by oxidative phosphorylation. Complexes I, III and IV drive protons into the inter-membrane space across the mitochondrial inner membrane, thus creating an electrochemical gradient across the inner membrane. ATP synthase, or Complex V, uses this gradient to make ATP from ADP and inorganic phosphate.

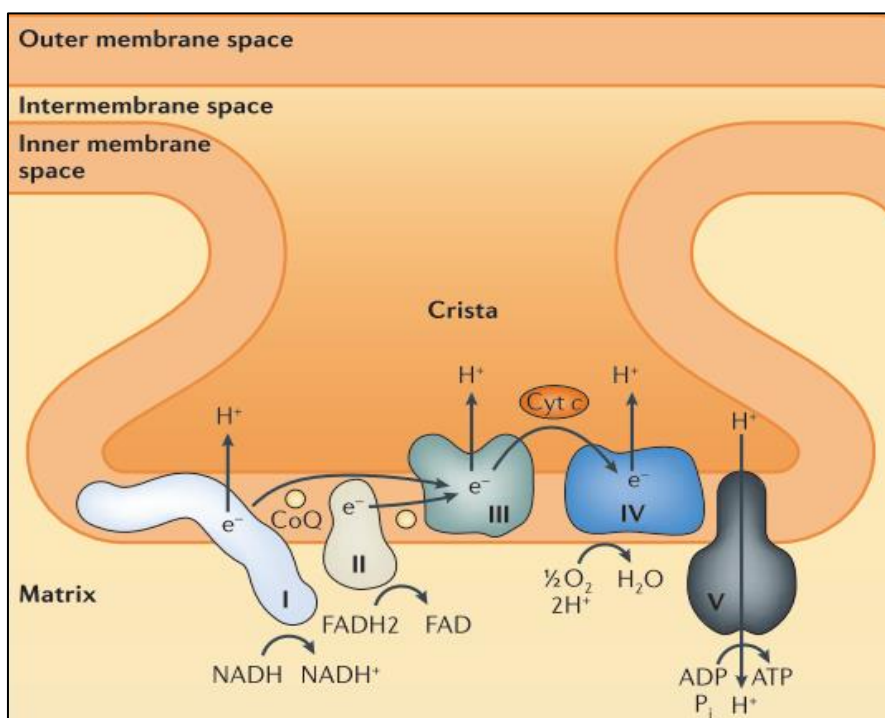


Figure 1.2: Schematic representation of the mitochondrial electron transport chain (Mishra and Chan, 2014)

Mitochondrial energetics intimately correlates with mitochondrial morphology – fused mitochondria are typically associated with higher cristae density, ATP production and enhanced calcium buffering, whereas fragmented mitochondria are considered to be metabolically less efficient with low ETC activity (Mishra and Chan, 2016). ETC functionality is also governed by cristae shape since membrane folding allows the formation of supercomplexes among ETC complexes I, III and IV, and dimerization of complex V, increasing metabolic output by the assembly of ETC hubs and increasing the accessibility of the ETC substrates within cristae pockets (Cogliati et al., 2013, 2016). Mitochondrial metabolism is also known to have an impact on cell differentiation. To illustrate, terminal stem cell differentiation in the *Drosophila* brain is facilitated by a shift in the metabolic profile of the cell from glycolysis to oxidative phosphorylation (Homem et al., 2014), orchestrated by steroid hormone signaling during the larval-to-pupal transition. Another report identified that the mitochondrial ATP synthase enzyme is necessary for the differentiation of germ stem cells in the *Drosophila* ovary independent of its function in ATP synthesis (Teixeira et al., 2015), for it promotes cristae maturation in the mitochondria by forming protein dimers and ETC supercomplexes

1.3. Interaction between mitochondria and signaling pathways

Mitochondria are known to partake in multiple signaling events within the cell such as the intrinsic cascade for apoptosis initiated by the release of cytochrome-c, and the shift in gene expression triggered by the mitochondrial production of ROS and stabilization of hypoxia-inducible factor (HIFs) in response to low oxygen environments (Chandel, 2014). Additionally, there exist detailed analyses that concentrate on how ROS signaling impacts stem cell homeostasis (Bigarella et al., 2014), but there are relatively few studies focussing on the importance of other physiological functions of mitochondria such as its morphology in self-renewing stem cells and their role in differentiation. Recently, studies have uncovered this aspect of mitochondrial function (Kasahara and Scorrano, 2014; Noguchi and Kasahara, 2017); for instance, mitochondrial fission mediated by Drp1 is essential for follicle cell differentiation during oogenesis in the *Drosophila melanogaster* ovary (Mitra et al.). Inhibition of mitochondrial fission in these cells causes excess cell proliferation and prevents Notch-mediated differentiation, resulting in developmental abnormalities. The EGFR pathway via Ras-ERK signaling maintains appropriate mitochondrial

membrane potential in follicle cells, and depletion of ERK in the fission-deficient background restores Notch activity and differentiation (Tomer et al., 2018). On another note, upregulation of the transcription factor Yorkie/YAP in *Drosophila* causes mitochondrial fusion by directly regulating the expression of fusion genes *marf* and *opa1* (Nagaraj et al., 2012). In the mammalian embryo, depletion of mitochondrial fusion proteins and subsequent mitochondrial fragmentation activates Notch1 signaling in embryonic stem cells due to sustained calcium signaling which hinders cardiomyocyte differentiation (Kasahara et al., 2013). Perturbation of mitochondrial dynamics also affects the transcriptional programme in neural stem cells in mammals, causing premature differentiation of stem cells (Khacho et al., 2016). Altogether, there is now increasing evidence to suggest that mitochondria play an active role in regulating the process of cell differentiation, opening up several unanswered questions in the cell biology field.

1.4. *Drosophila* neuroblasts as a model to study mitochondrial functions during cell differentiation

Neuroblasts in *Drosophila* are primarily defined in the developing embryo and these stem cells proliferate through the embryonic and larval stages of development (Homem and Knoblich, 2012). NBs are first formed in the neuroepithelium of the early embryo via lateral inhibition, when cell-to-cell communication refines gene expression to define cell fate. The Notch-Delta signaling pathway acts to increase the expression of proneural genes in certain discrete cells. These neural stem cells delaminate from the neuroepithelium and gradually start dividing to generate neurons and glia that constitute the central nervous system. There exist two waves of neurogenesis during *Drosophila* development – the first wave consists of divisions of embryonic NBs to produce neurons that constitute the central nervous system (CNS) of the developing larva. Embryonic NBs enter a state of quiescence after the first round of proliferation. Concomitant with larval hatching, NBs re-enter mitosis and the second wave of neurogenesis begins from the first instar larval stage. This wave contributes to the formation of neurons that constitute the adult brain. The four major types of NBs – type-I, type-II, mushroom body and optic lobe NBs can be distinguished based on their positions in the brain and characteristic lineages. Type-I and type-II NBs are located in the central brain region of each lobe in the larval brain, medial to the optic lobe. Nearly 85-90 type-I NBs are distributed among the anterior

and posterior side of the brain, and exactly 8 type-II NBs and their lineages are found on the posterior side of the larval brain. Type-I NBs undergo asymmetric division to form a ganglion mother cell (GMC) that divides to generate two post-mitotic differentiated cells (Fig.1.3A). On the contrary, type-II NBs go through a series of asymmetric divisions to generate intermediate neural progenitors (INPs) (Bello et al., 2008; Boone and Doe, 2008; Bowman et al., 2008), which go through a maturation step by initiating transcriptional changes. Mature INPs are characterized by the expression of transcription factors Asense, Deadpan and Prospero, and have a unique property of transit amplification. They continue to divide asymmetrically around 3-5 times to produce another mature INP and a GMC (Fig.1.3B) which distinguishes type-II lineages from type-I lineages. GMCs then divide to generate two post-mitotic neurons or glial cells. On the whole, transit amplification allows for the production of a large number of differentiated cells from a limited number of progenitors.

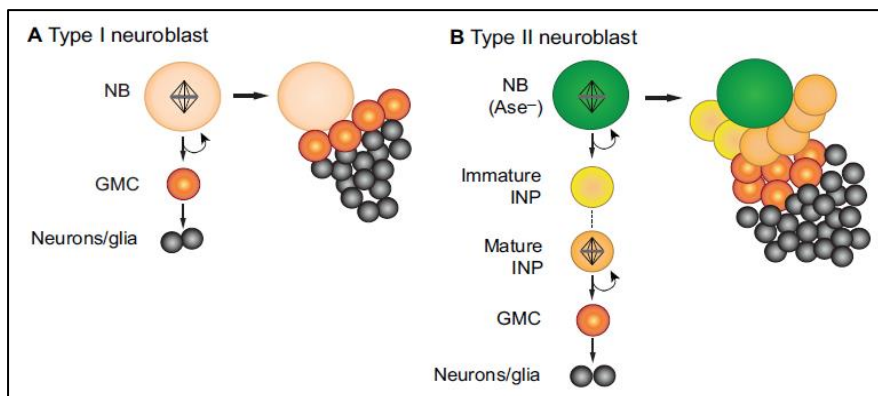


Figure 1.3: Asymmetric cell division in central-brain *Drosophila* neuroblasts. Lineage progression in (A) type-I neuroblasts and (B) type-II neuroblasts. (Homem and Knoblich, 2012)

1.5. Notch signaling in *Drosophila* neuroblasts

Notch signaling maintains the *Drosophila* neuroblasts in a proliferative state and is indispensable for self-renewal of the stem cell pool (Wang et al., 2006). The Notch pathway is then inhibited in the smaller daughter cell formed during neuroblast asymmetric division by segregation of the Notch inhibitor Numb. This promotes expression of neural genes and subsequent differentiation in the daughter cell, directing it towards the INP or GMC state. *Drosophila* has two Notch ligands that are single-pass transmembrane proteins, namely Delta and Serrate (Bray, 2006). Ligand-binding activates the Notch receptor and results in sequential proteolytic cleavage steps – ADAM-family metalloproteases first cleave the Notch extracellular domain (NECD), followed by γ -secretase activity which releases the Notch

intracellular domain (NICD)(Bray, 2006)(Bray, 2006) (Bray, 2006) (Fig.1.4). NICD has a nuclear localization sequence that guides it to the nucleus, where it forms a part of a protein complex along with co-activators CBF1, Suppressor of Hairless Su(H), LAG-1 (CSL complex) and Mastermind (Mam) to regulate gene expression of its targets. The Enhancer of split [E(spl)] locus is one of the primary Notch signaling targets, which encodes basic helix-loop-helix (bHLH) transcription factors that determine cell fate.

Additionally, a non-canonical Notch pathway involving mitochondria also contributes to neuroblast self-renewal, wherein Notch interacts with PTEN-induced putative kinase-1 (PINK1) to stimulate activation of mTORC2/AKT signaling in tumor-forming stem cells (Lee et al., 2013). However, it remains unexplored whether Notch, a pre-requisite for neuroblast proliferation in *Drosophila*, is associated with mitochondrial morphology in stem cells.

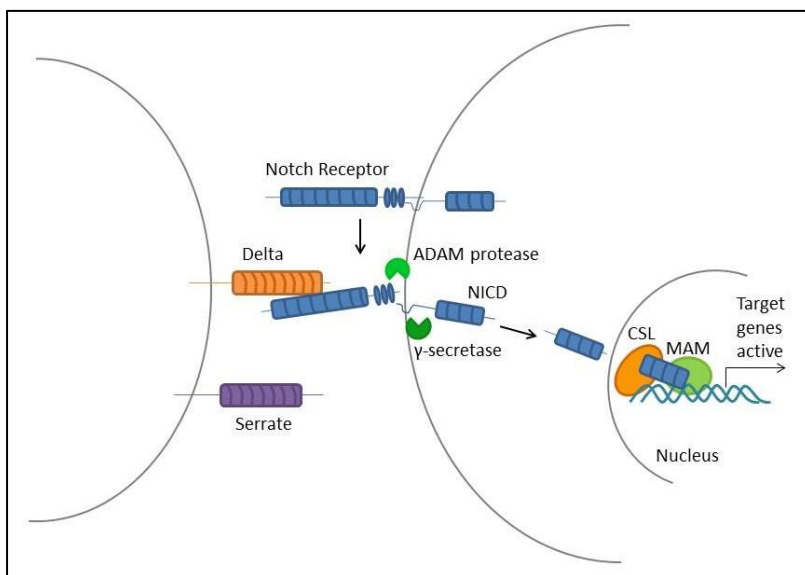


Figure 1.4: Summary of the canonical Notch signaling pathway: Delta and Serrate are Notch ligands that bind to the transmembrane Notch receptor, which triggers cleavage of the Notch receptor. The Notch intracellular domain (NICD) is released, and it enters the nucleus to regulate gene expression along with transcriptional co-activators CSL complex and Mastermind (Mam).

1.6. Objectives

Altogether, the primary focus of my project is to study the role of mitochondrial functions, mainly dynamics and metabolism, in regulating differentiation of type-II neuroblasts. I will explore the nature of the interaction between mitochondria and signaling pathways such as Notch in maintaining a mitochondrial architecture that is conducive for stem cell proliferation and differentiation. I will focus on the lineage-specific analysis type-II neuroblast differentiation as this system has similarities to vertebrates regarding the cell and molecular biology of neural stem cell self-renewal

and differentiation (Brand and Livesey, 2011). The objectives of my study are as follows:

- Study of neuroblast differentiation in response to perturbing mitochondrial dynamics by targeting effector proteins, allowing analysis of the dependence of the neuroblast differentiation program on mitochondrial architecture.
- Analysis of differentiation defects in mutants for electron transport chain activity to elucidate whether defects in ETC function and differentiation are mechanistically related.
- Examining the role of Notch signaling in mediating the mitochondrial morphology and metabolism during differentiation of neuroblasts.
- Studying the role of reactive oxygen species (ROS) and calcium signaling in driving the loss of neuroblast differentiation on alteration of mitochondrial morphology and metabolism.

2. Materials and methods

2.1. *Drosophila* stocks and crosses

All *Drosophila* crosses were performed in standard cornmeal agar medium at 29°C. The *Drosophila* Canton-S strain was used as control. The UAS-Gal4 system in *Drosophila* was used for targeted knockdown of proteins. The promoter of the type-II NB specific gene *pointed* was used for tissue-specific Gal4 expression and subsequent RNAi-mediated knockdown of target genes during development. Fly stocks were obtained from the Bloomington *Drosophila* Stock Centre, unless stated otherwise. The lines used in the project are as follows: *pntGal4* UAS-mCD8GFP (gift from Jurgen Knoblich Lab), *opa1ⁱ* (BL32358), *opa1^{miRNA}* (BL67159), *marfⁱ* (gift from Ming Guo Lab), *marfⁱ* (BL31157), *covaⁱ* (BL27548), *atpbⁱ* (BL28056), *notchⁱ* (BL31383), *suhⁱ* (BL67928), *importinⁱ* (BL27535), UAS-Notch (BL52309) and UAS-*N_{intra}* (gift from LS Shashidhara Lab). The Drp1 mutant line expressing UAS-Drp1^{SD} (Drp1 protein with a point mutation S193D in the GTPase domain) was previously generated in the lab. Double mutant combination stocks were made using standard genetic crosses.

2.2. Immunostaining

Wandering third instar larvae were collected from crosses maintained at 29°C and their brains were dissected at room temperature in Schneider's Medium supplemented with serum. Dissected brains of one genotype and the corresponding control were stained in the same tube by trimming the ventral nerve cord (VNC) of control brains to distinguish them from mutant brains. After dissection, the brains were immediately fixed for 25 minutes in 4% paraformaldehyde. After fixation, brains were washed once for 30 minutes with 1x PBS and 0.1% Triton-X (1xPBST). Blocking was carried out at room temperature by incubating the brains in 1% BSA in 1xPBST and then incubated in primary antibody overnight at 4°C. Next, the brains were washed with 1xPBST for 20 minutes followed by two washes of 10 minutes each and incubated for 1 hour at room temperature in secondary antibody. After washing the brains in PBST for 20 minutes, Hoechst was added for 6 minutes to label DNA, followed by a final wash with 1xPBST for 10 minutes. The brains were mounted on a glass slide with their ventral side down and dorsal side facing up in ProLong Gold Antifade mountant (Thermo Fischer Scientific) for confocal

microscopy, or in Mowiol-DABCO stock solution for super-resolution (STED) microscopy.

Table 2.1: List of antibodies and dyes used in the project

Primary Antibody	Dilution	Source
anti-GFP	1:1000	Invitrogen
anti-ATP β	1:100	Abcam
anti-Deadpan	1:150	Abcam
anti-Prospero	1:25	DSHB
anti-Miranda	1:200	Chris Doe Lab; Abcam
anti-Elav	1:10	DSHB
anti-Cytochrome-c	1:200	Cell Signalling
anti-NICD	1:10	DSHB
anti-Cleaved Notch	1:10	Cell Signalling
Anti-Su(H)	1:50	Santa Cruz
anti-pAMPk	1:200	Cell Signalling
anti-Cleaved Caspase-3	1:100	Cell Signalling
anti-pH3	1:1000	Invitrogen
Anti- γ H2Ax	1:1000	Bethyl Laboratories
Secondary Antibody		
Alexa488	1:1000	Invitrogen
Alexa568	1:1000	Invitrogen
Alexa633	1:1000	Invitrogen
Dyes		
Hoechst	1:1000	Invitrogen, 20mM stock
DHE	1:1000	Invitrogen

2.3. Manipulation of cellular functions using pharmacological treatment

2.3.1. Depolarization of mitochondria using FCCP

Third instar larval brains were first dissected in Schneider's medium supplemented with serum and then incubated in 10 μ m carbonilcyanide p-triflouromethoxyphenylhydrazone (FCCP, Sigma Aldrich) for 30 minutes. 10mM FCCP stock was made in 100% ethanol. After drug treatment, the brains were fixed with 4% formaldehyde for 25 minutes, followed by the standard immunostaining protocol mentioned in section 2.2 to probe for mitochondrial morphology and markers intermediates of the Notch signaling pathway.

2.3.2. Inhibition of glycolysis using 2-DG

Fly cages were set up with *pntGal4* male and female flies at 25°C. Embryos were collected over an 8-hour window and incubated overnight at 25°C. Larval hatching was synchronized by collecting larvae that hatched within a 2-hour window 22 hours after egg-laying. First instar larvae were transferred to standard cornmeal agar medium and maintained at 25°C. For the feeding experiment, third instar larvae were selected 120 hours after larval hatching (AHL) and incubated in 3ml yeast paste supplemented with 500uM 2-deoxyglucose (2-DG) for 2 hours (10mM stock in DMSO). Control larvae were incubated in yeast paste with DMSO for 2 hours. After feeding, larval brains were dissected in Schneider's medium supplemented with serum followed by the standard immunostaining protocol mentioned in section 2.2 to probe for pAMPk antibody to analyse AMPk activation.

2.4. Microscopy

2.4.1 Imaging of fixed samples using confocal microscopy

Confocal microscopy for fixed samples was done at room temperature (21°C) using LSM-710 or LSM-780 inverted microscope (Carl Zeiss, Inc. and IISER Pune microscopy facility) with a Plan apochromat 63x/1.4NA oil objective. The Alexa Fluor fluorophores 488, 568 and 633 were excited with 488nm, 561nm and 633nm lasers and emission was collected with PMT filters. Images were acquired using the Zen2011 software at 1024x1024 pixels, with an averaging of 4 and acquisition speed 7. Fluorescence intensity was kept within 255 on an 8-bit scale using the range indicator mode to avoid over-saturated pixels. A zoom of 2 was used to image an entire type-II NB lineage, and a zoom of 4 was used to image individual type-II NBs. Z-stacks were acquired such that all the GFP-marked daughter cells of a type-II NB lineage were visible, with z-stack interval 0.8um.

2.4.1. Super-resolution microscopy using Stimulated Emission-Depletion

Super-resolution microscopy was done to resolve mitochondrial structure within type-II NBs using the Leica TCS SP8 STED 3X Nanoscope with a 100x/1.4NA oil objective. Images were acquired using the LasX software at 1024x1024 pixels to keep pixel size between 20-25nm, with an averaging of 4 and acquisition speed 200. The Alexa Fluor fluorophores 488 and 568 were excited with 488nm, and 561nm lasers and emission was collected with hybrid detectors. The 561nm excitation laser

with the 775nm depletion laser was used for stimulated emission-depletion. Fluorescence intensity was kept within 255 on an 8-bit scale using the LUT mode to avoid over-saturated pixels. A zoom of 4.5 was used to image mitochondrial morphology in individual type-II NBs.

2.4.2. Measurement of ROS using DHE and live imaging

Third instar larval brains were first dissected in Schneider's medium supplemented with serum and incubated in 30nM DHE in Schneider's for 15 minutes. The brains were then washed for 10 minutes with Schneider's medium and transferred to a LabTek chamber. The brains were placed with their dorsal side facing down, and fresh media was added such that the brains remain submerged to allow live imaging of the sample to visualize changes in ROS. Live images were acquired using Zeiss LSM 710 with a 63x/1.4NA oil objective under the dihydroethidium-1 channel settings in the Zeiss2010 software.

2.5. Image analysis and statistics for cell counting and fluorescence estimation

Differentiated cells in each type-II NB lineage were analyzed using the Cell Counter module in ImageJ; cells expressing a nuclear Deadpan signal were counted as mature INPS, those with a nuclear Prospero signal were counted as GMCs. Quantification of pAMPk, Cytochrome-c, cleaved Notch, Suppressor of Hairless, γ H2Ax and membrane NICD fluorescence intensity for WT and mutants was also performed using ImageJ. Fluorescence intensity was measured by selecting a region of interest (ROI) using GFP/Miranda as markers of cell boundary and Hoechst staining for nuclear signals. Appropriate normalization of the intensity values was done to account for imaging conditions as described. Normalization for pAMPk and cytochrome-c intensity was done by taking the ratio of mean intensity in the NB to the mean intensity over an identical ROI in differentiated cells of the lineage. For cleaved Notch, the ratio of nuclear-to-cytoplasmic mean intensity was used for analysis. Likewise, the mean nuclear intensity of γ H2Ax was normalized by its mean cytoplasmic signal. Quantification of membrane-enriched NICD fluorescence intensity for WT, *cova*ⁱ, FCCP-treatment and corresponding EtOH control was calculated using a segmented line of thickness 20 points drawn along the plasma membrane of type-II NBs using GFP and Miranda as markers of the cell boundary. Mean fluorescence intensity of NICD was measured along the membrane, and it was

divided by mean cytoplasmic intensity of NICD within the type-II NB for normalization across samples. GraphPad Prism was used to plot graphs and perform statistical analyses. Two-tailed, unpaired student's *t*-test was performed to compare the number of differentiated cells and normalized fluorescence intensity among different genotypes.

3. Results

3.1. Depletion of Marf and Opa1 decreases mitochondrial fusion and depletion of Drp1 increases mitochondrial fusion in *Drosophila* type-II neuroblasts

Mitochondria exist as a fine, tubular network in *Drosophila* type-II neuroblasts (NBs) (Fig.3.1A), and inhibition of either mitochondrial fusion or fission alters mitochondrial morphology. RNAi-mediated depletion of Marf (*marfⁱ*) and Opa1 (*opa1ⁱ*) in type-II NBs abolished the thread-like mitochondrial network observed in wild-type NBs (Fig.3.1B, C). Instead, mitochondria appeared distinctly fragmented in the mutants (as evaluated by immunostaining with an antibody against ATPsyn β , a protein on the inner mitochondrial membrane) and had a swollen morphology. We validated the ATP β antibody by checking that the signal is lost upon RNAi-mediated depletion of ATP β (Appendix Fig.A1). Likewise, we observed severely fused mitochondria on the Gal4-driven expression of a Drp1 mutant, namely *drp1^{S193D}* (*drp1^{SD}*), in the type-II NBs (Fig.3.1D). The point mutation is in the GTPase domain of Drp1, and we predict that it behaves as a dominant negative allele by inactivating the endogenous Drp1 protein to form an aggregated mitochondrial cluster.

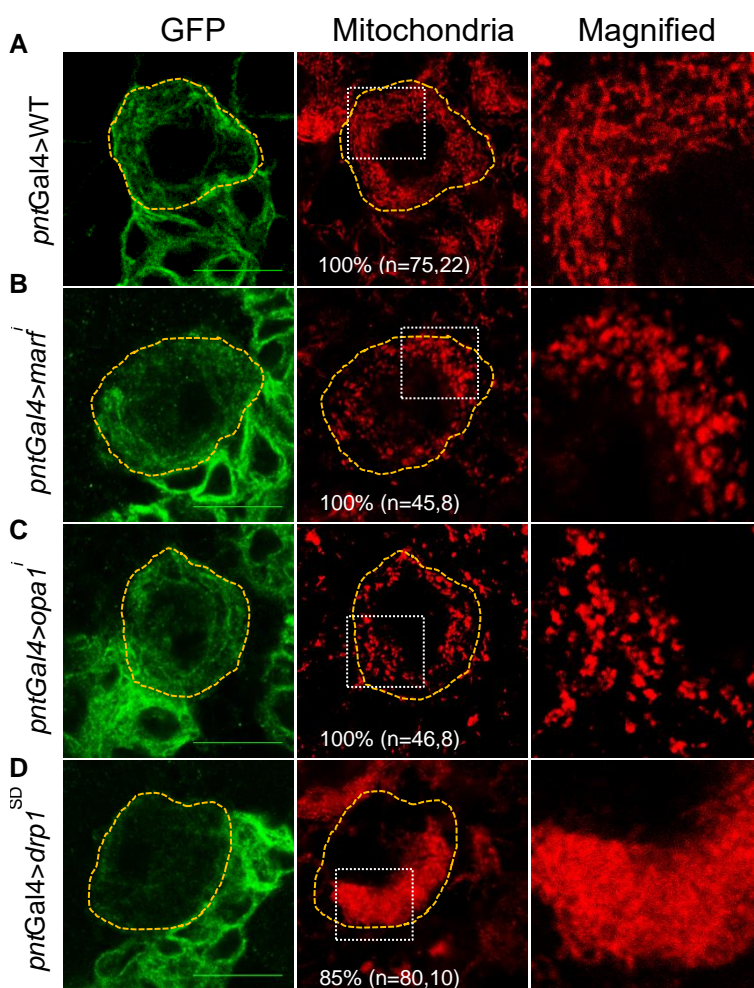


Figure 3.1: Depletion of Marf and Opa1 decreases mitochondrial fusion and depletion of Drp1 increases mitochondrial fusion in *Drosophila* type-II neuroblasts. Super-resolution STED images of mitochondrial morphology in type-II NBs of (A)WT, (B)*marfⁱ*, (C)*opa1ⁱ* and (D)*drp1^{SD}* mutants. Yellow dotted outline represents NB cell boundary, areas marked by white squares are magnified in the right panels. Percentage indicates frequency of the observed phenotype out of n= (number of NBs, number of brain lobes) type-II NBs recorded. Scale bar = 10 μ m.

3.2. Inhibition of mitochondrial fusion in *marf* and *opa1* results in a decrease in the number of differentiated cells in the type-II neuroblast lineage

We proceeded to analyze the effect of disruption of mitochondrial morphology on NB proliferation and differentiation. Firstly, the number of type-II NBs in each lobe of the third instar larval brain in *marf*, *opa1*, and *drp1^{SD}* mutants was unchanged; there were always exactly eight type-II NBs per lobe in each of the mutants (Fig.3.2E). We then analyzed the *marf*, *opa1* and *drp1^{SD}* mutant NBs for lineage progression by evaluating different cell types present in each lineage, such as mature INPs that express transcription factor Deadpan (Dpn) and GMCs that show nuclear Prospero (Pros). It was evident that inhibition of mitochondrial fusion decreased the differentiation of type-II NBs. We observed a minor increase in the number of mature INPs in the lineage upon Marf depletion (Fig.3.2B, F), whereas Opa1 depletion caused a significant decrease in the number of mature INPs compared to wild-type (Fig.3.2C, F). Further, both *marf* and *opa1* lineages exhibited a prominent decrease in the number of GMCs in the lineage (Fig.3.2B', C', G). This combined effect led to a decrease in the lineage size in *opa1* mutants compared to the size of control lineages primarily due to the decrease in the GMC population. Despite having a common function of facilitating mitochondrial fusion, these results suggest that Marf and Opa1 have varying roles in regulating proteins that bring about the proliferation of the NBs. Notably, forced mitochondrial fusion in the NB in *drp1^{SD}* mutants did not affect NB proliferation and differentiation (Fig.3.2 D,D'), and lineage progression is comparable to wild-type NBs (Fig.3.2F, G).

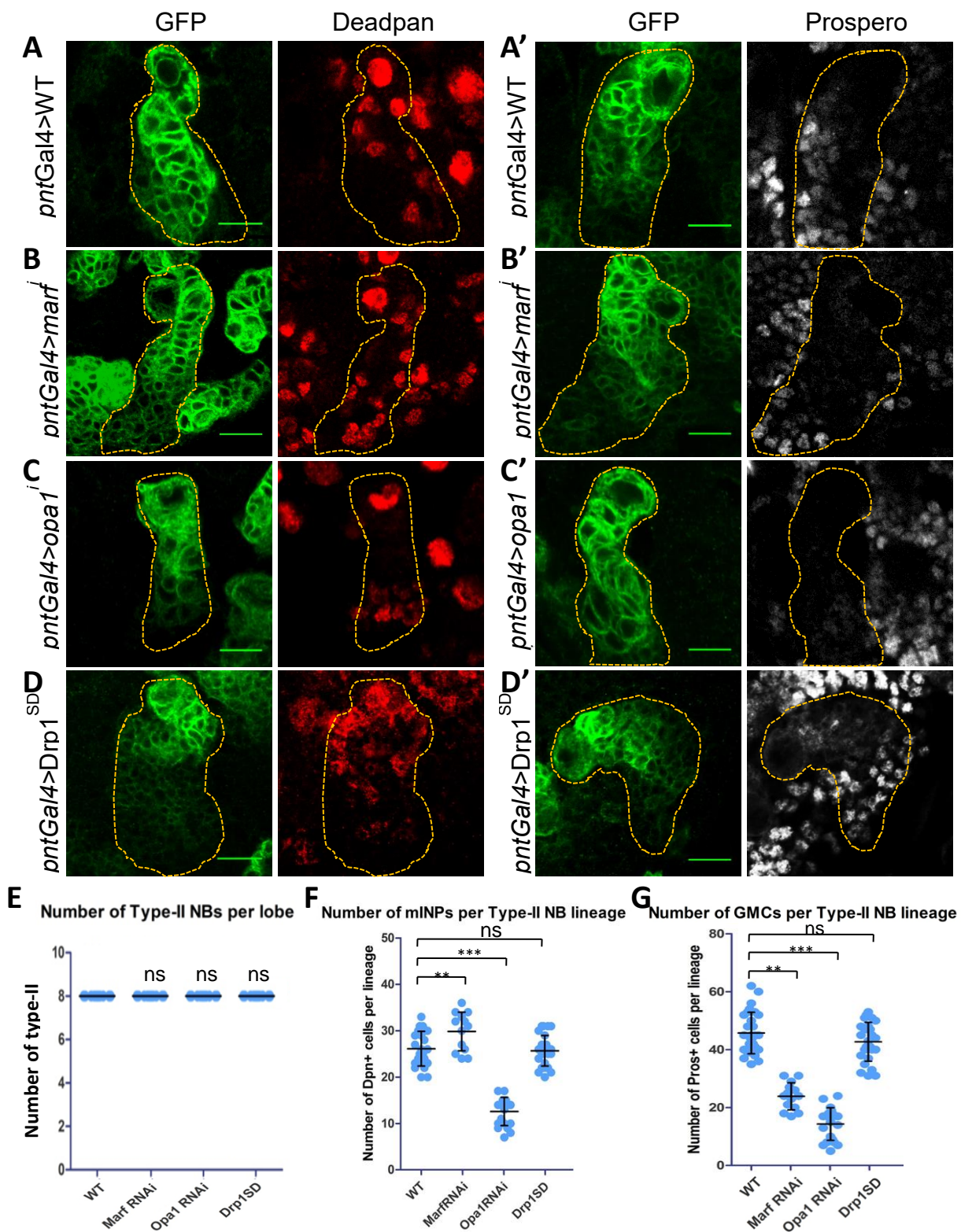


Figure 3.2: Inhibition of mitochondrial fusion in *marf* and *opa1* results in a decrease in the number of differentiated cells in the type-II neuroblast lineage.

(A-D) Analysis of type-II NB lineages for (A) WT, (B) *marf* (C) *opa1*ⁱ and (D) *drp1*^{SD} mutants for differentiation using mature INP-specific marker Deadpan. (A'-D') Analysis using GMC-specific marker Prospero. (E) Quantification for number of type-II NBs per lobe in WT, *marf*ⁱ, *opa1*ⁱ, and *drp1*^{SD} mutants. n=(30,15) for all genotypes. (F) Quantification for mature INP analysis in (A-D). n=(23,16) for WT, (13,6) for *marf*ⁱ, (20,8) for *opa1*ⁱ and (28,10) for *drp1*^{SD}. (G) Quantification for number of GMCs per lineage in (A'-D'). n=(29,18) for WT, (14,6) for *marf*ⁱ, (20,8) for *opa1*ⁱ and (26,8) for *drp1*^{SD}. Scale bar = 10µm. Analysis was done using an unpaired t-test. ns=non-significant, **=*p*<0.01, ***=*p*<0.001.

3.3. Forced mitochondrial fusion by inhibition of *drp1*-mediated fission in *marf* and *opa1* background rescues the loss of differentiated cells in the type-II neuroblast lineage

To check whether the defect observed in NB differentiation on inhibiting mitochondrial fusion is solely dependent on mitochondrial morphology, we forced mitochondrial fusion in *marf* and *opa1* mutants by inhibiting mitochondrial fission in this background. We expressed *drp1*^{SD} in the background of *marf*ⁱ and *opa1*ⁱ and observed that the mitochondrial cluster was slightly resolved (Fig3.A, B), and the loss of NB differentiation was also alleviated. We expressed RFP in the background of *drp1*^{SD} to account for Gal4 dilution and confirmed that mitochondrial morphology was as clustered as the *drp1*^{SD} mutant alone (Fig.3.3C, and Appendix Fig.3. A3). The number of mature INPs in the *marf* and *opa1* type-II NB lineages was similar to control (Fig.3.3D, E, F), but the GMC population was not restored (Fig.3.3G, H, I), resulting in only partial rescue of the phenotype. In summary, inhibiting mitochondrial fission in the background of Marf or Opa1 depletion enables fused mitochondrial morphology even in the absence of mitochondrial fusion, and this partially rescues the number of differentiated cells in the *marf* and *opa1* lineages. In the *drp1*^{SD}; *marf* double mutant, the number of mature INPs is comparable to WT and the number of GMCs also increases compared to the *marf* lineage alone, although GMC numbers do not increase to WT levels. In the *drp1*^{SD}; *opa1*ⁱ combination, forced mitochondrial fusion facilitates production of mature INPs from the type-II NB but does not improve the formation of GMCs from mature INPs.

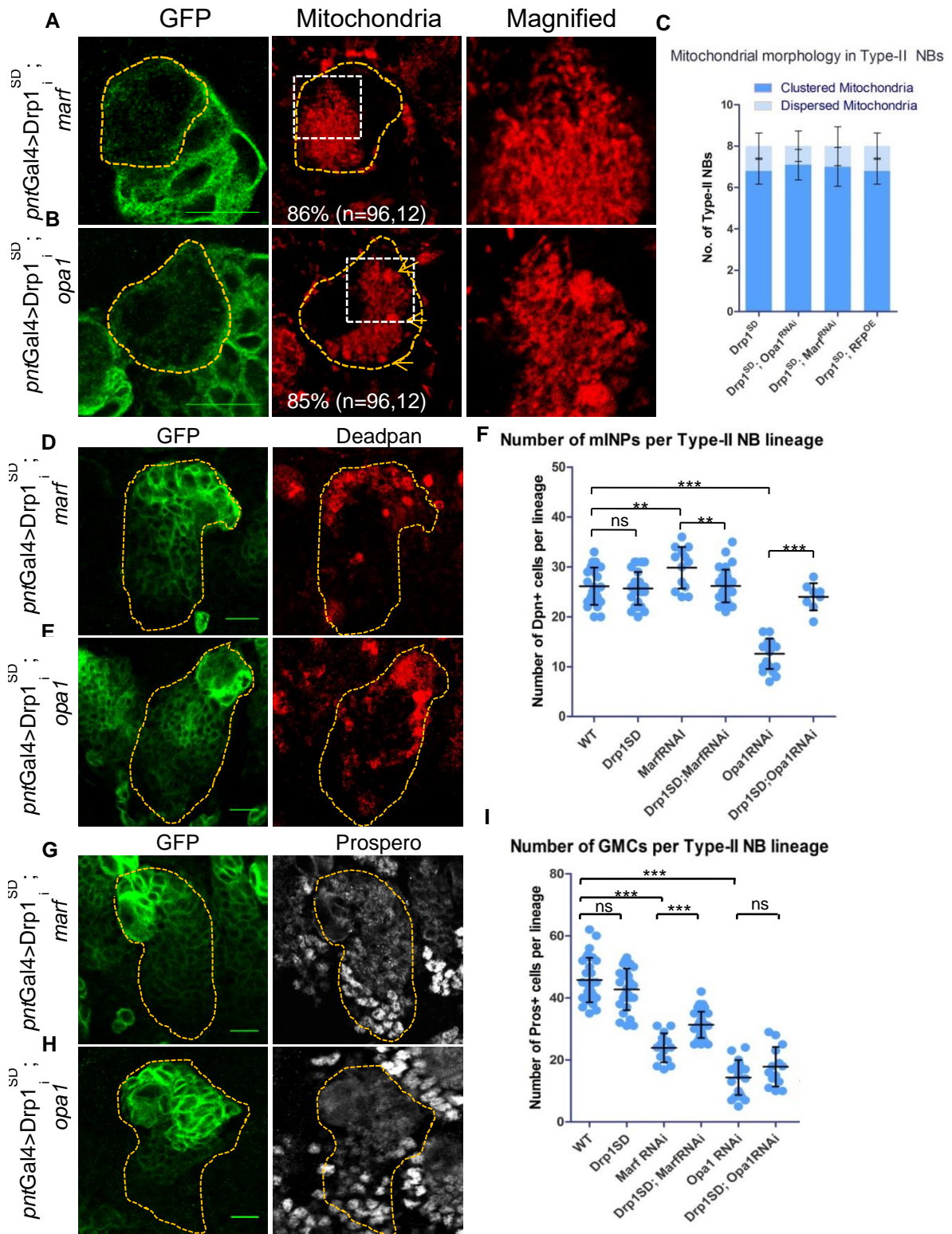


Figure 3.3: Forced mitochondrial fusion by inhibition of *drp1*-mediated fission in *marf* and *opa1* background rescues the loss of differentiated cells in the type-II neuroblast lineage.

(A,B) Super-resolution STED images for mitochondrial morphology in type-II NBs of $drp1^{SD}; marf$ and $drp1^{SD}; opa1$ mutants respectively. Percentages indicate the frequency of the observed phenotype out of n=(number of NBs, number of brain lobes) type-II NBs recorded. (C) Quantification of the number of type-II NBs showing clustered vs. dispersed mitochondria on $drp1^{SD}$ expression. (D,E) Immunostaining with Deadpan (Dpn) for number of mature INPs in the type-II NB lineage of $drp1^{SD}; marf$ and $drp1^{SD}; opa1$ mutants. (F) Analysis for (D) and (E) compared to single mutants.

n=(23,16) for WT, (28,10) for *drp1^{SD}*, (13,6) for *marfⁱ*, (35,8) for *drp1^{SD};marfⁱ*, (20,8) for *opa1ⁱ* and (8,6) for *drp1^{SD};opa1ⁱ*. (G,H) Immunostaining with Prospero (Pros) for number of GMCs in the type-II NB lineage of *drp1^{SD};marfⁱ* and *drp1^{SD};opa1ⁱ* mutants. (I) Analysis for (G) and (H) compared to single mutants. n=(29,18) for WT, (26,8) for *drp1^{SD}*, (14,6) for *marfⁱ*, (33,8) for *drp1^{SD};marfⁱ*, (20,8) for *opa1ⁱ* and (14,8) for *drp1^{SD};opa1ⁱ*. Scale bar = 10 μ m. Statistical significance was calculated using an unpaired *t*-test. ns=non-significant, **= p <0.01, ***= p <0.001.

3.4. Cellular effects of inhibition of mitochondrial fusion in *marf* and *opa1*

3.4.1. Analysis of cell cycle, apoptosis and DNA damage on depletion of *marf* and *opa1* in type-II neuroblasts

The decrease in the population of differentiated cells per lineage in *marf* and *opa1* mutants could either be due to slower cell divisions or increased cell death within the lineage. To understand how the lineage size decreased in the mitochondrial dynamics mutants we tried to estimate cell division rate in the cells of the type-II NB lineage by probing with phospho-histone H3 (Hans and Dimitrov, 2001). Depletion of Marf did not significantly affect the number of cells in mitosis in the lineage (Fig.3.4.1A, B) whereas Opa1 depletion reduces the number of pH3-positive cells in the type-II NB lineage (Fig.3.4.1A, B). This suggested that inhibition of mitochondrial fusion by downregulating Opa1 decreases cell cycle rate. Additionally, we checked for cell death by immunostaining for cleaved caspase-3 in the *opa1* mutant since its phenotype is stronger compared to the *marf* mutant. Cleaved caspase-3 was not upregulated within the cells of the *opa1* mutant lineage, as the immunostaining was observed to be similar in the type-II NB lineages in WT and *opa1* mutants (Fig.3.4.1C), indicating that apoptosis was not the cause of decreased lineage size. Further, we checked whether the slower rate of the cell cycle was due to cell-cycle arrest induced by DNA damage within the NBs. We examined DNA damage by immunostaining with γ H2Ax, which is a histone variant that accumulates on DNA in case of double-stranded breaks (Paull et al., 2000). We analyzed the nuclear intensity of γ H2Ax in the NBs, which revealed no significant change in its expression (Fig.3.4.1D,E).

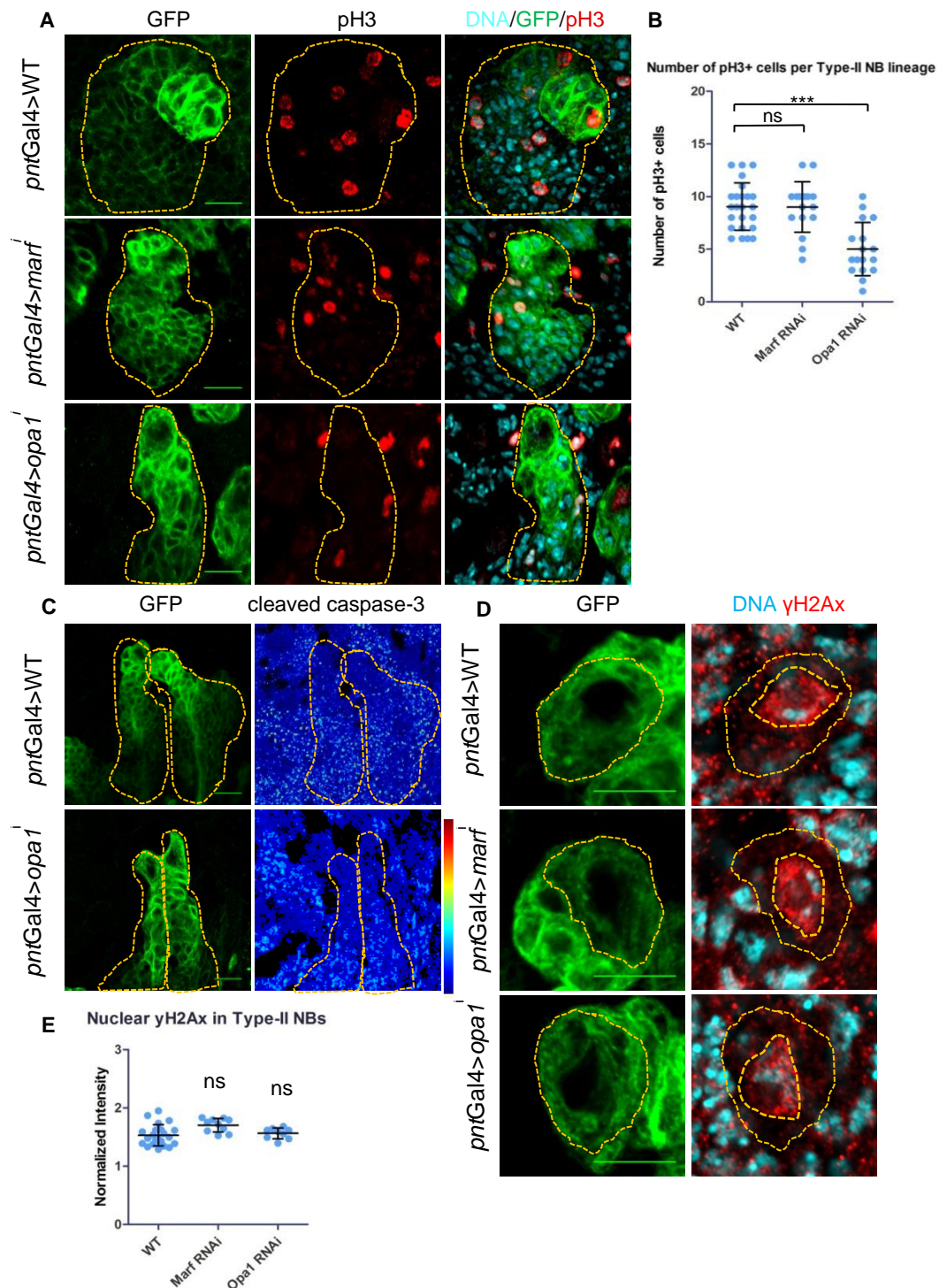


Figure 3.4.1: Cellular effects of inhibition of mitochondrial fusion in *marf* and *opa1*.

Inhibition of mitochondrial fusion in *marf* and *opa1* decreases mitotic cells in the NB lineage, does not induce apoptosis and does not increase γ H2Ax in the type-II NBs.

(A) Analysis of type-II NB lineages for cells in mitosis by phospho-histone H3 (pH3) staining in WT, *marf*ⁱ and *opa1*ⁱ. Yellow dotted outline represents NB lineage boundary. (B) Quantification of number of mitotic cells per lineage represented in (A). n=(28,16) for WT, (17,6) for *marf*ⁱ and (17,4) for *opa1*ⁱ. (C) Cleaved caspase-3 expression represented as a heat map in WT (n=10,6) and *opa1*ⁱ (n=9,6) brains, blue regions indicate low intensity and red indicate high intensity. (D) Analysis of type-II NB for γ H2Ax in WT, *marf*ⁱ, and *opa1*ⁱ. Yellow dotted outline represents NB cell, and nucleus boundary was marked using GFP and Hoechst. (E) Quantification of γ H2Ax signal intensity represented in (D). n=(22,12) for WT, (10,6) for *marf*ⁱ and (9,6) for *opa1*ⁱ. Scale bar = 10 μ m. Analysis was done using an unpaired t-test. ns=non-significant, **= p <0.01, ***= p <0.001

3.4.2. Analysis of mitochondrial activity in the form of pAMPK, cytochrome-c and ROS levels on depletion of *marf* and *opa1* in type-II neuroblasts

To understand the mechanism that decreases NB differentiation and lineage size upon inhibition of mitochondrial fusion we explored its cellular effects in the type-II NBs. We first investigated whether fragmented mitochondria in *marf* and *opa1* caused an energy-deficient condition for the NB by immunostaining against the phosphorylated form of adenosine monophosphate-activated protein kinase (p-AMPk). AMPk is activated via phosphorylation when the ATP level in a cell is low; its activation then stops biosynthetic pathways and promotes catabolism to generate energy for cellular functions (Hardie et al., 2012). Interestingly, AMPk was not activated in type-II NBs in *marf* and *opa1* mutants, indicating that the NBs do not experience a shortage of ATP (Fig.3.4.2A,B). The neuroblasts in the larval brain primarily depend on glycolysis for ATP generation (Homem et al., 2014), and when glycolysis was inhibited by feeding larvae with 2-deoxyglucose (2-DG), an increase in the pAMPk signal was observed in the brain (Fig.3.4.2B,F), suggesting that energy stress leads to the activation of AMPk in this context.

Since Opa1 is known to maintain the stability of cristae pockets of the inner mitochondrial membrane which houses proteins of the electron transport chain (Cogliati, Scorrano; Cell, 2016), we examined whether cristae structure is affected on inhibition of mitochondrial fusion. We used cytochrome-c as a read-out for cristae stability as it is known to get mobilized on disruption of cristae pockets (Frezza et al., 2006; Scorrano, 2009). Indeed, we observed that cytochrome-c substantially increases in the type-II NBs upon depletion of Opa1 (Fig.3.4.2C,D). After analyzing the ratio of cytochrome-c expression in the type-II NBs compared to differentiated cells (normalized intensity in Fig.3.4.2D), we noted that this ratio for WT was higher than 1.0, indicating that the expression of cytochrome-c within the NB per se was higher than differentiated cells. We also checked the status of reactive oxygen species by live-imaging brains treated with the ROS-specific dye dihydroethidium (DHE). It was evident that ROS increases upon inhibition of mitochondrial fusion (Fig.3.4.2E). However, DHE staining displayed a punctate pattern in type-II NBs in *marf* mutants, suggesting that ROS might be trapped within the mitochondria. In contrast, we observed a marked increase in ROS in *opa1* mutants not only in the type-II NBs but also in the daughter cells of the NB in the lineage (Fig.3.4.2E).

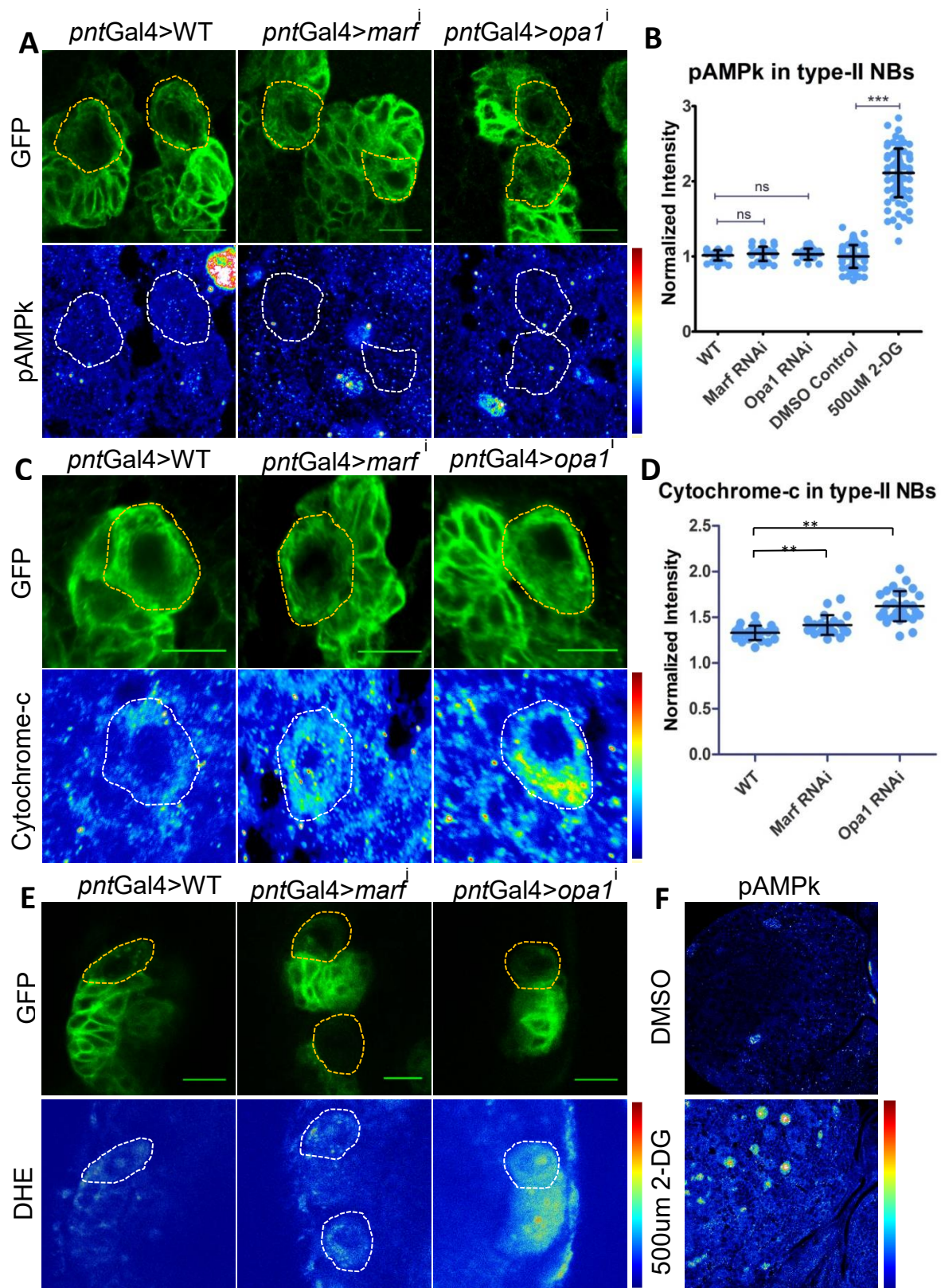


Figure 3.4.2: Cellular effects of inhibition of mitochondrial fusion in *marf* and *opa1*.

Inhibition of mitochondrial fusion in *marf* and *opa1* increases cytochrome-c and ROS in the type-II NBs. (A) Analysis of type-II NB for activation of AMPk in WT (n=41,14), *marfⁱ* (n=33,8) and *opa1ⁱ* (n=23,8). pAMPk intensity represented as heat-map, blue indicates low intensity and red indicates high intensity on the heat-map scale. (B) Quantification of pAMPk signal intensity represented in (A) with positive control for the antibody on 2-DG feeding (n=45,12) and corresponding DMSO control (n=30,10). (C) Cytochrome-c expression represented as a heat map in WT (n=31,18), *marfⁱ* (n=10,6)

and *opa1*ⁱ (n=20,12). (D) Quantification for cytochrome-c fluorescence intensity in (C). (E) DHE staining for reactive oxygen species (ROS) in type-II NBs of WT, *marf*ⁱ and *opa1*ⁱ brains. n= (34,14) for WT, (10,6) for *marf*ⁱ and (30,8) for *opa1*ⁱ. Yellow and white dotted outline represents NB cell boundary. (F) Analysis for activation of AMPK by phosphorylation in the brain upon larval feeding with 500uM 2-DG in the absence of glucose and corresponding DMSO control; pAMPK staining represented as a heat map. Scale bar = 10µm. Analysis was done using an unpaired t-test. ns=non-significant, **= $p < 0.01$, ***= $p < 0.001$.

Altogether, depletion of mitochondrial fusion proteins decreases the number of mitotic cells in the lineage and results in an increase in cytochrome c and ROS within the type-NB. We next assessed whether the known Notch signaling pathway involved in type-II NB proliferation could interact with mitochondrial morphology.

3.4.3. Notch signaling is abrogated in type-II neuroblasts depleted of Marf and Opa1
A non-canonical Notch signaling axis that participates in NB self-renewal and involves mitochondria was previously reported in a tumor model in *Drosophila* NBs (Lee et al., 2013). This led us to explore the effect of inhibiting mitochondrial fusion on Notch signaling in type-II NBs. Canonical Notch signaling functions via ligand-dependent cleavage of the transmembrane Notch receptor to release the intracellular domain (NICD) (Bray, 2006). NICD then translocates into the nucleus and interacts with specific transcription factors in complex to regulate target gene expression. We examined the localization of the cleaved Notch intracellular domain (cleaved NICD) by immunostaining to assess Notch signaling activity within type-II NBs upon mitochondrial perturbation. The antibody is specific for the domain of NICD exposed after its cleavage from the Notch receptor on the membrane and marks the nuclear fraction of NICD specifically (Cho et al., 2017). Immunostaining shows clear nuclear localization of cleaved NICD in control type-II NBs (Fig.3.4.3A). Depletion of Marf and Opa1 and the following fragmented mitochondrial state resulted in the cytoplasmic accumulation of cleaved NICD (Fig.3.4.3A). After analyzing the nuclear-to-cytoplasmic intensity ratio of cleaved-NICD the type-II NBs, it became clear that the ratio decreased in *marf* and *opa1* mutants compared to wild-type, specifically due to a high cytoplasmic signal (Fig.3.4.3B). Additionally, we analyzed *marf*ⁱ and *opa1*ⁱ with an antibody against NICD and detected its cytoplasmic accumulation in *opa1*ⁱ only (Appendix Fig.A2).

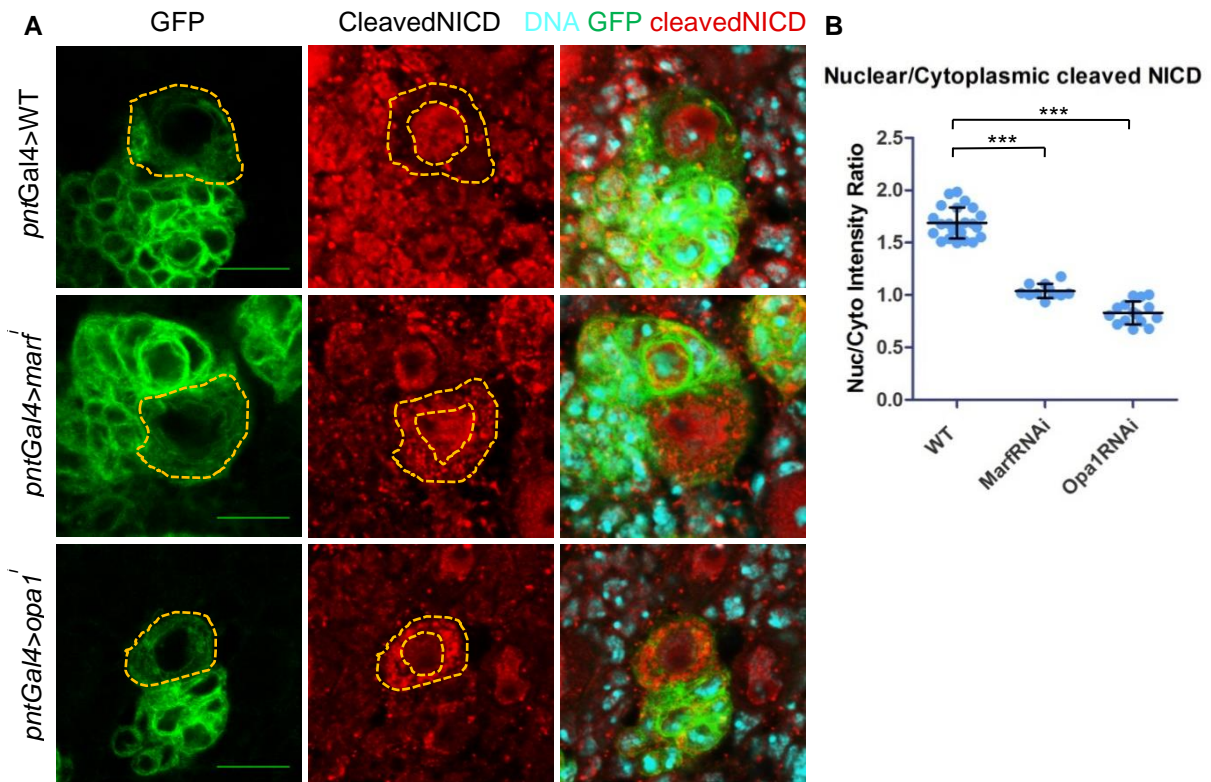


Figure 3.4.3: Cellular effects of inhibition of mitochondrial fusion in *marf* and *opa1*.

Inhibition of mitochondrial fusion in *marf* and *opa1* causes cytoplasmic accumulation of cleaved NICD in type-II NBs. (A) Cleaved NICD localization in type-II NBs in WT, *marf*ⁱ and *opa1*ⁱ brains. Yellow dotted outline represents NB cell and nucleus boundary. (B) Quantification of cleaved NICD fluorescence intensity represented as nuclear/cytoplasmic intensity ratio from (A). n= (40,18) for WT, (12,6) for *marf*ⁱ and (16,6) for *opa1*ⁱ. Scale bar = 10µm. Analysis was done using an unpaired *t*-test. ns=non-significant, **=*p*<0.01, ***=*p*<0.001.

3.5. Notch signaling maintains fused mitochondria in the type-II neuroblasts

Notch signaling is responsible for maintaining the NBs in a proliferative state and is necessary for their self-renewal (Wang et al., 2006). Since depletion of Marf and Opa1 resulted in the cytoplasmic accumulation of NICD, it could inhibit the downstream nuclear transcriptional program if NICD is sequestered in the cytoplasm. Therefore, we increased expression of the full-length Notch receptor in type-II NBs to evaluate whether increased signaling activity rescued the lineage size and differentiation. However, it resulted in hyperproliferation of type-II NBs, since they are sensitive to changes in Notch signaling (Zacharioudaki et al., 2012). Depletion of Marf or Opa1 in the Notch overexpression background alleviated the Notch-mediated hyper-proliferation of type-II NBs (Fig.3.5.1A, B). Interestingly, mitochondria in the NBs seemed more fused and gathered towards one side of the cell when Notch was overexpressed alone (Fig.3.5.2B), suggesting that Notch could play a role in maintaining a fused mitochondrial network in the NB. We then upregulated NICD

expression to bypass the receptor cleavage step and checked mitochondrial morphology. Although NICD overexpression caused type-II NB hyperproliferation at the expense of differentiation, remarkably, mitochondrial fusion increased upon constitutively activating the Notch pathway such that mitochondria were clustered to one side of the NB (Fig.3.5.2C). This fusion is Marf- and Opa1-dependent, since mitochondria remained fragmented when we depleted these proteins in the active Notch signaling background (Fig.3.5.2D,E), despite NICD being entirely in the nucleus (Fig.3.5.1F). Also, inhibition of mitochondrial fusion in the NICD overexpression background alleviated Notch-mediated type-II NB hyperproliferation (Fig.3.5.1C,D). We hypothesized that Notch signaling acts upstream of mitochondrial dynamics to promote fusion through its ability to regulate gene expression.

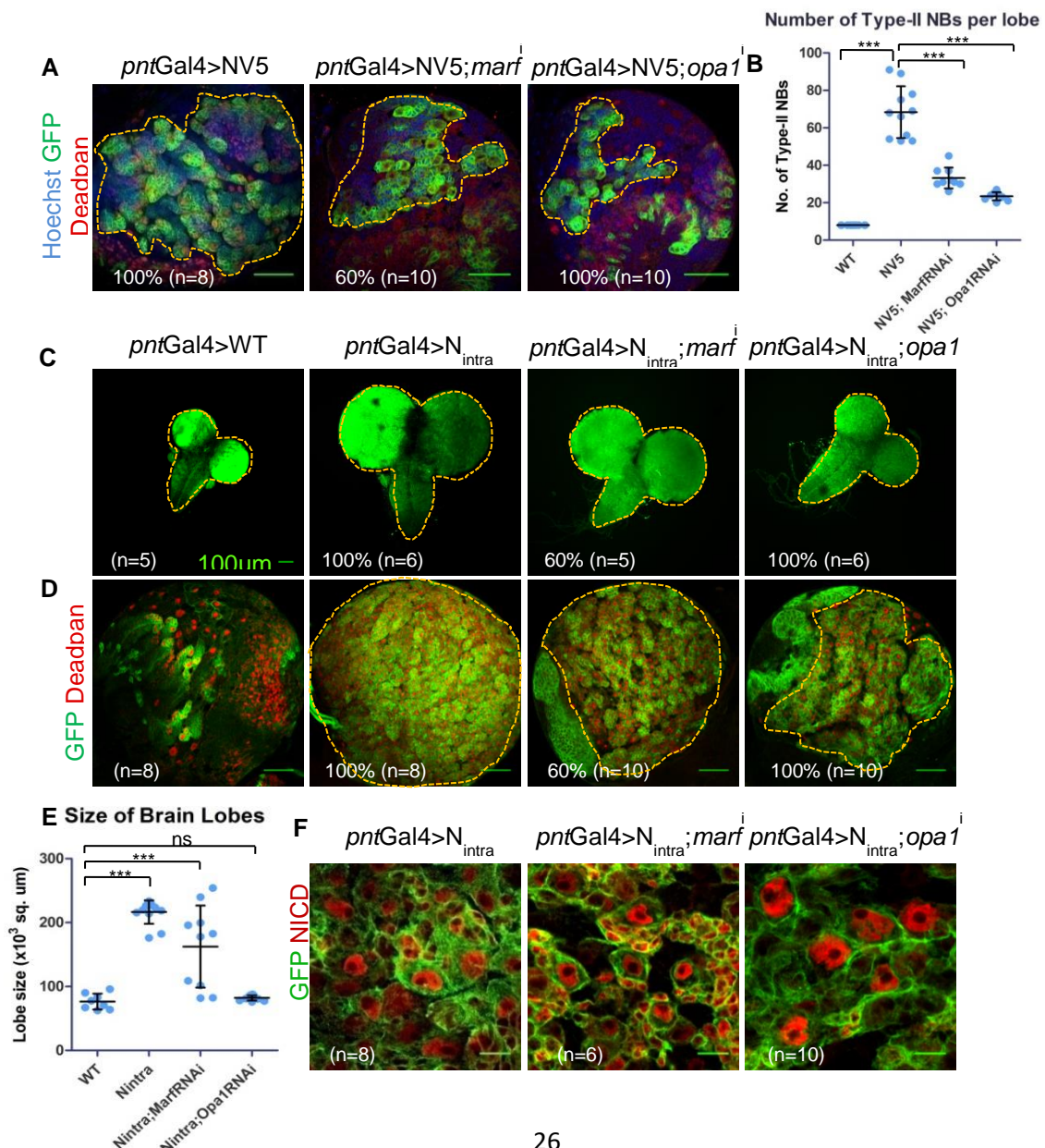


Figure 3.5.1: Depletion of Marf and Opa1 alleviates Notch-mediated type-II NB hyperproliferation.

(A) Analysis of type-II NB hyperproliferation upon overexpression of the full-length Notch receptor (NV5), UAS-NV5;*marf*^{-/-} and UAS-NV5;*opa1*^{-/-}. Yellow dotted lines mark type-II NB proliferation zone positive for GFP and Deadpan. Scale bar = 50µm. (B) Quantification of number of type-II NBs per lobe represented in (A). (C) Representation of WT, UAS-N_{intra}, UAS-N_{intra};*marf*^{-/-} and UAS-N_{intra};*opa1*^{-/-} brains. Yellow dotted lines mark the boundary of the brain. (D) Notch-mediated type-II NB hyperproliferation upon overexpression of the Notch intracellular domain (N_{intra}); yellow dotted lines mark proliferation zone positive for both GFP and Deadpan. Scale bar = 50µm. (E) Quantification of brain lobe size of WT, UAS-N_{intra}, UAS-N_{intra};*marf*^{-/-} and UAS-N_{intra};*opa1*^{-/-} brains from (C). Percentage indicates the frequency of the observed phenotype out of n= (number of brains) recorded. Scale bar = 10µm. Analysis was done using an unpaired *t*-test. ns=non-significant, **=*p*<0.01, ***=*p*<0.001.

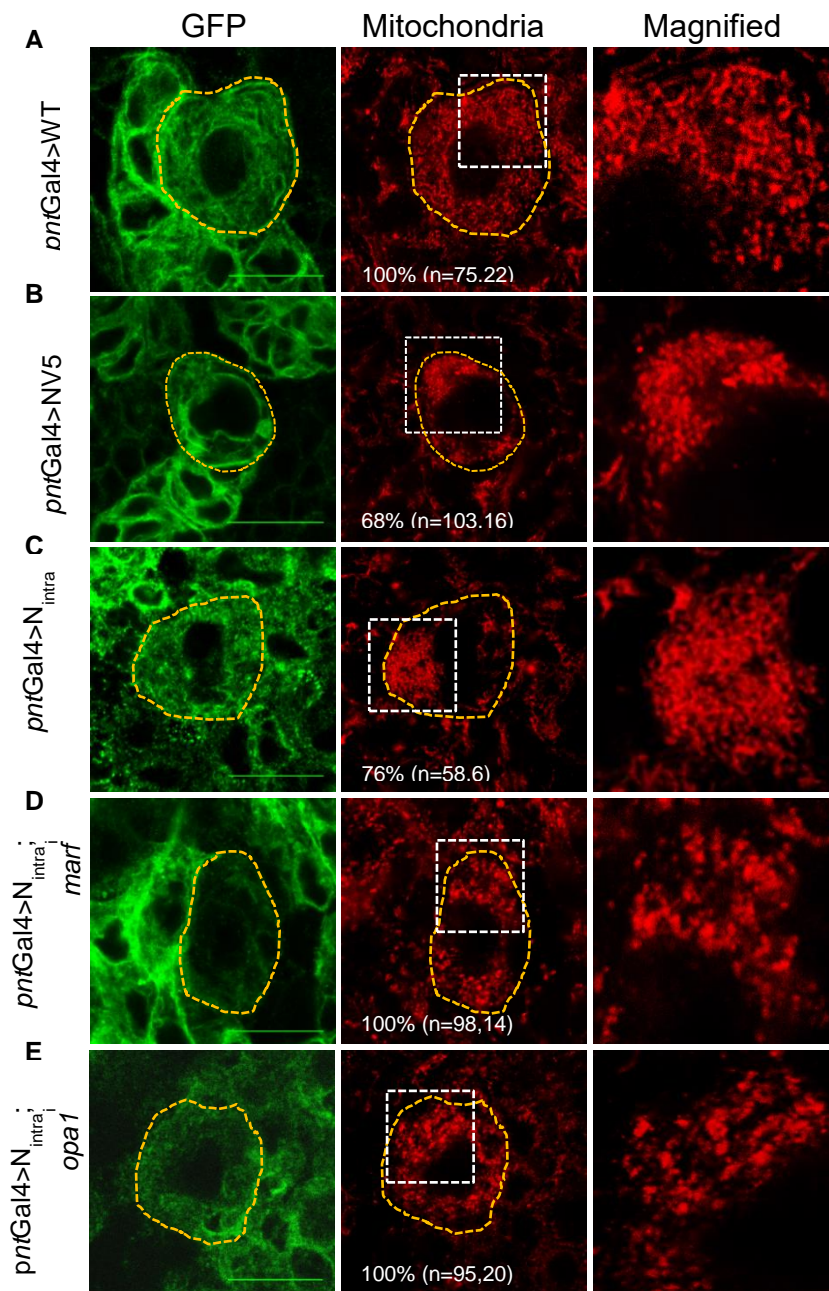


Figure 3.5.2: Notch signaling maintains a fused mitochondrial morphology in type-II neuroblasts.

Super-resolution STED images of mitochondrial morphology type-II NBs in (A) WT, (B) overexpression of full-length Notch receptor (NV5), (C) overexpression of the Notch intracellular domain (N_{intra}), (D) UAS-N_{intra};*marf*^{-/-} and (E) UAS-N_{intra};*opa1*^{-/-} brains. Yellow dotted lines mark NB cell boundary, areas marked by white squares are magnified in the right panels. Percentage indicates frequency of the observed phenotype out of n= (number of NBs, number of brain lobes) type-II NBs recorded. Scale bar = 10µm.

Furthermore, we analyzed mitochondrial morphology in response to decreased Notch activity. Downregulation of Notch in type-II NBs is known to reduce overall NB numbers in the brain (Bowman et al., 2008) (Fig.3.5.3B). RNAi-mediated depletion of Notch resulted in fragmented mitochondrial morphology (Fig.3.5.3A) (Refer to Fig. 3.1A and 3.1D for mitochondrial morphology in WT NBs and NBs expressing *drp1^{SD}* respectively). We confirmed that Notch signaling reduces in *notch* mutants by analyzing the nuclear localization of cleaved Notch in the mutants, and indeed, quantification of nuclear intensity revealed that it was lower compared to WT (Fig.3.5.3C,D). Likewise, depletion of intermediate transcription factors of the Notch pathway such as Suppressor of Hairless (Su(H)) in type-II NBs also resulted in fragmented mitochondrial morphology. This is consistent with the hypothesis that Notch is capable of regulating mitochondrial dynamics by modulating the expression of fusion proteins.

Once we observed that mitochondria are fragmented upon downregulation of Notch signaling, we analysed mitochondrial morphology upon forcing fusion using *drp1^{SD}*. Mitochondria were clustered in the *drp1^{SD}; notchⁱ* double mutants, as fused as mitochondria in NBs with *drp1^{SD}* expression alone (Fig.3.5.4A) and this did not affect the number of type-II NBs per lobe compared to Notch loss of function mutants (Fig.3.5.4B). We then proceeded to analyse mINP and GMC differentiation in the type-II NB lineage and observed that the lineage size in *notchⁱ* mutants was small, and had fewer Dpn+ mature INPs and Pros+ GMCs in the lineage compared to WT. We then assessed whether forcing mitochondrial fusion by expressing *drp1^{SD}* in the background of lowered Notch signaling was capable of rescuing differentiation. Forced mitochondrial fusion in *notchⁱ* background was indeed able to rescue differentiation and these brains had larger type-II NB lineages owing to an increase in the number of mature INPs than *notchⁱ* mutants (Fig.3.5.4C,D) and an increase in GMCs compared to *notchⁱ* mutants (Fig.3.5.4E,F). In summary, it appears that mitochondrial fusion downstream of Notch activity allows for NB proliferation and the subsequent production of differentiated cells in the type-II NB lineage.

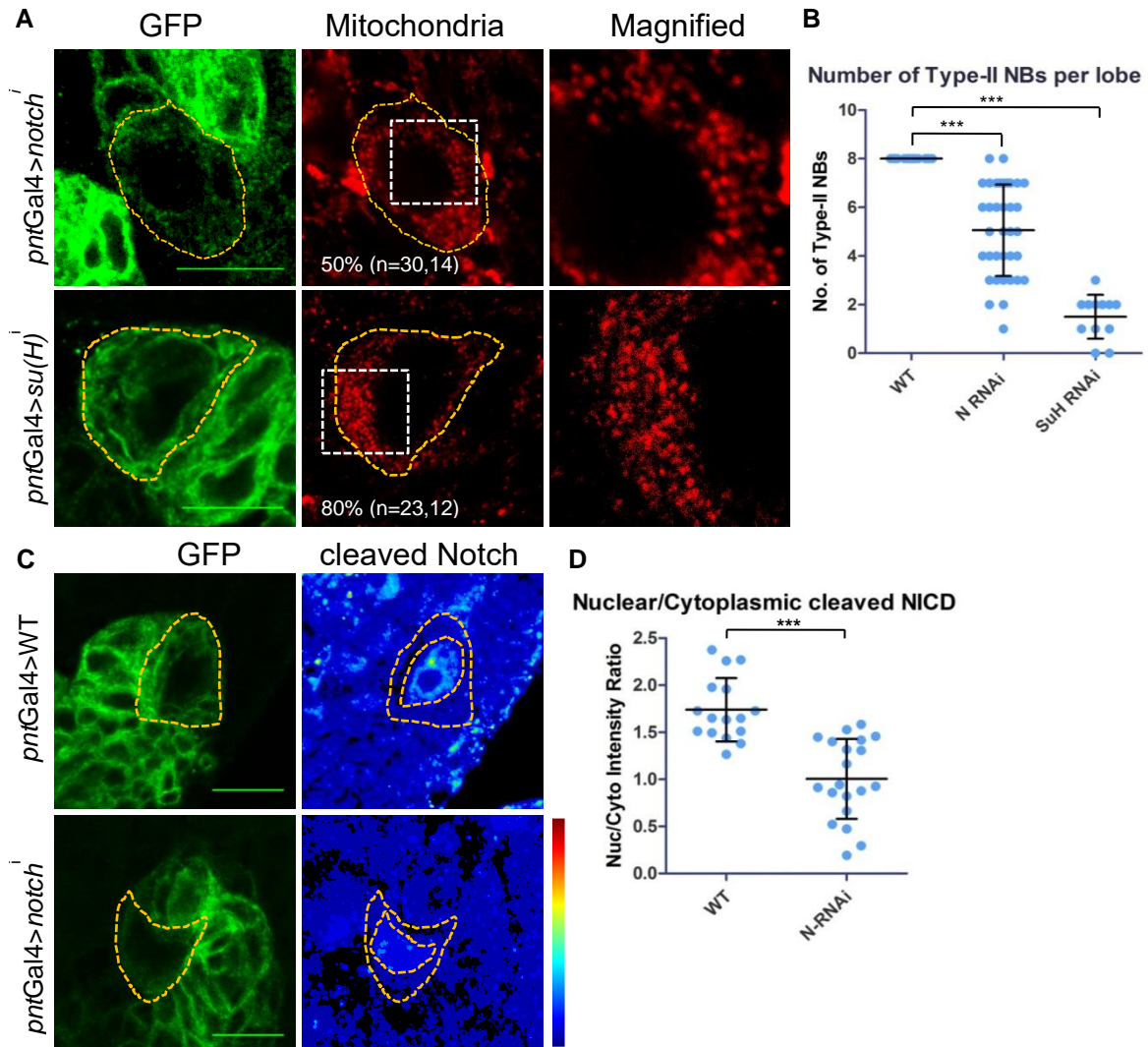


Figure 3.5.3: Notch signaling maintains fused mitochondria in type-II neuroblasts.

(A) Super-resolution images of mitochondrial morphology type-II NBs upon RNAi-mediated depletion of Notch and Suppressor of Hairless Su(H). Yellow dotted lines mark NB cell boundary, areas marked by white squares are magnified in the right panels. Percentage indicates the frequency of the observed phenotype out of n= (number of NBs, number of brain lobes) type-II NBs recorded. Refer to Fig. 3.1A and 3.1D for mitochondrial morphology in WT NBs and NBs expressing *drp1^{SD}* respectively. (B) Quantification of number of type-II NBs per lobe in *notchⁱ* and *su(H)ⁱ*. n=(15,30) for WT, n=(34,17) for *notchⁱ* and n=(12,6) for *su(H)ⁱ*. (C) Cleaved NICD localization in type-II NBs in WT, *notchⁱ* brains, cleaved NICD intensity represented as a heat-map, with blue marking regions of low intensity and red depicting high intensity. Yellow dotted lines mark NB cell boundary and nucleus. (D) Quantification of cleaved NICD fluorescence intensity represented as nuclear/cytoplasmic intensity ratio from (C). n=(16,8) for WT and (20,8) for *notchⁱ*. Scale bar = 10 μ m. Analysis was done using an unpaired *t*-test. ns=non-significant, **= $p < 0.01$, ***= $p < 0.001$.

3.6. Analysis of inhibition of the mitochondrial electron transport chain on mitochondrial morphology and differentiation of type-II NBs

3.6.1. Depletion of ETC ComplexIV decreases the number of differentiated cells in the type-II neuroblast lineage

It is well-known that mitochondrial morphology and metabolism are inter-connected, with fused mitochondria typically associated with higher cristae density and ATP output; and fragmented mitochondria linked to poor cristae structure and low ATP output (Mishra Chan 2014). Therefore, we analyzed mitochondrial morphology in response to inhibition of the mitochondrial electron transport chain. We examined mitochondrial morphology after RNAi-mediated depletion of subunit Va of ComplexIV (*cova*), and surprisingly, mitochondria remained fused in the form of connected thread-like structures (Fig.3.6.1A).

RNAi-mediated depletion of *cova* in type-II NBs did not change the number of type-II NBs in each lobe (Fig.3.6.1B) but resulted in a decrease in the differentiated cell population in the lineage (Fig.3.6.1C-F). Similar to the mitochondrial morphology mutants, a decrease in the number of mINPs and GMCs was observed, concomitant with a decrease in the number of mitotic cells in the type-II NB lineage (Fig.3.6.1G,H).

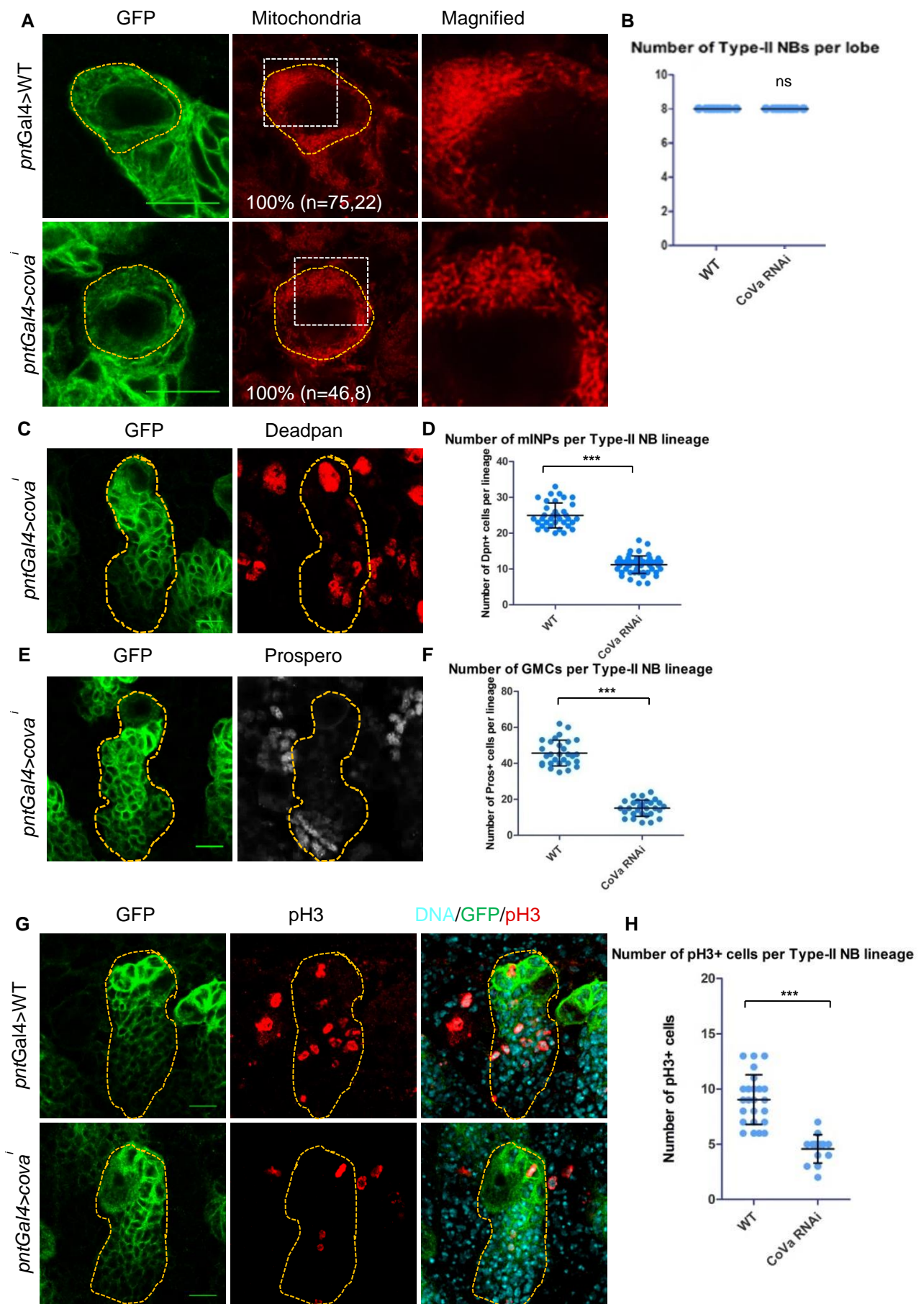


Figure 3.6.1: Inhibition of ETC in type-II neuroblasts causes differentiation defects in *cova* mutants.

(A) Super-resolution STED images of mitochondrial morphology type-II NBs upon RNAi-mediated depletion of subunit Va of ETC ComplexIV (CoVa). Yellow dotted lines mark NB cell boundary, areas marked by white squares are magnified in the right panels. Percentages indicate the frequency of the observed phenotype out of n =(number of NBs, number of brain lobes) type-II NBs recorded. (B) Quantification of number of type-II NBs per lobe in *cova*ⁱ. (C-F) Analysis of differentiation defects in *cova* mutants. Immunostaining with Deadpan (Dpn) (C) and Prospero (E) to analyze number of mature INPs and GMCs respectively in the type-II NB lineage of *cova*ⁱ mutants. (D) Quantification for number of mature INPs per type-II NB lineage from (C). n =(40,16) for WT and (62,10) for *cova*ⁱ. (F) Quantification for number of GMCs per type-II NB lineage from (E). n =(30,18) for WT and (29,10) for *cova*ⁱ. (G) Analysis for number of cells in mitosis per lineage in *cova* mutants by staining for phospho-histone H3, and (H) quantification number of pH3+ cells from (G). n =(28,16) for WT and (14,8) for *cova*ⁱ. Scale bar = 10 μ m. Analysis was done using an unpaired *t*-test. ns=non-significant, **= p <0.01, ***= p <0.001.

Inhibition of ETC did not result in the activation of AMPk (Fig.3.6.2A), suggesting that the NBs do not experience ATP shortage, since they primarily depend on glycolysis for ATP generation and not OxPhos (Homem et al., 2014). However, the *cova* mutant differed from the mitochondrial dynamics mutants regarding changes in ROS levels upon mitochondrial perturbation. Interestingly, depletion of *cova* in the NB resulted in a decrease in ROS in the type-II lineage (Fig.3.6.2B), which is in stark contrast with the ROS status in *marf* and *opa1* mutants. Additionally, there was no change in the expression of cytochrome-c in type-II NBs upon depletion of CoVa (Fig.3.6.2C,D), but NICD was marginally enriched on the membrane compared to WT, without any cytoplasmic accumulation of NICD (Fig.3.6.2E,F).

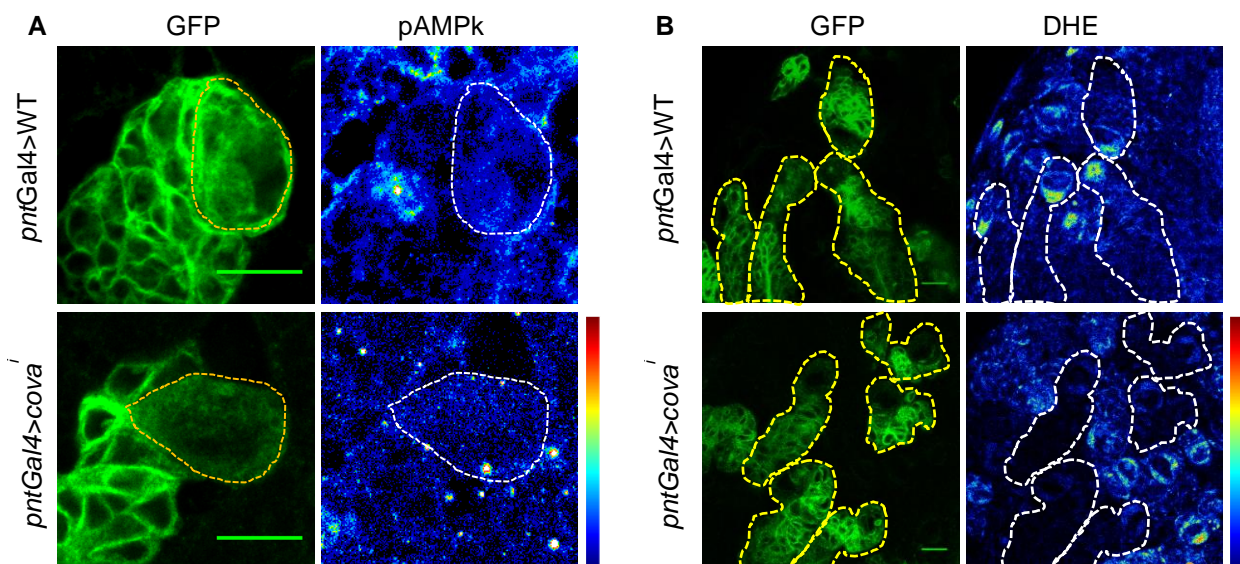


Figure 3.6.2: Inhibition of ETC in type-II neuroblasts decreases ROS and does not affect cytochrome-c in *cova* mutants.

(A) Analysis of type-II NB for activation of AMPk in WT and *cova*ⁱ mutants. pAMPk intensity represented as heat-map, blue indicates low intensity and red indicates high intensity on the heat-map scale. n =(33,14) for WT and (39,10) for *cova*ⁱ. Dotted lines mark type-II NB cell boundary. (B) DHE staining for reactive oxygen species (ROS) in type-II NBs of WT, *cova*ⁱ brains, represented on a heat-map scale. n =(34,14) for WT and (26,10) for *cova*ⁱ. Dotted lines mark the GFP-expressing type-II NB lineages.

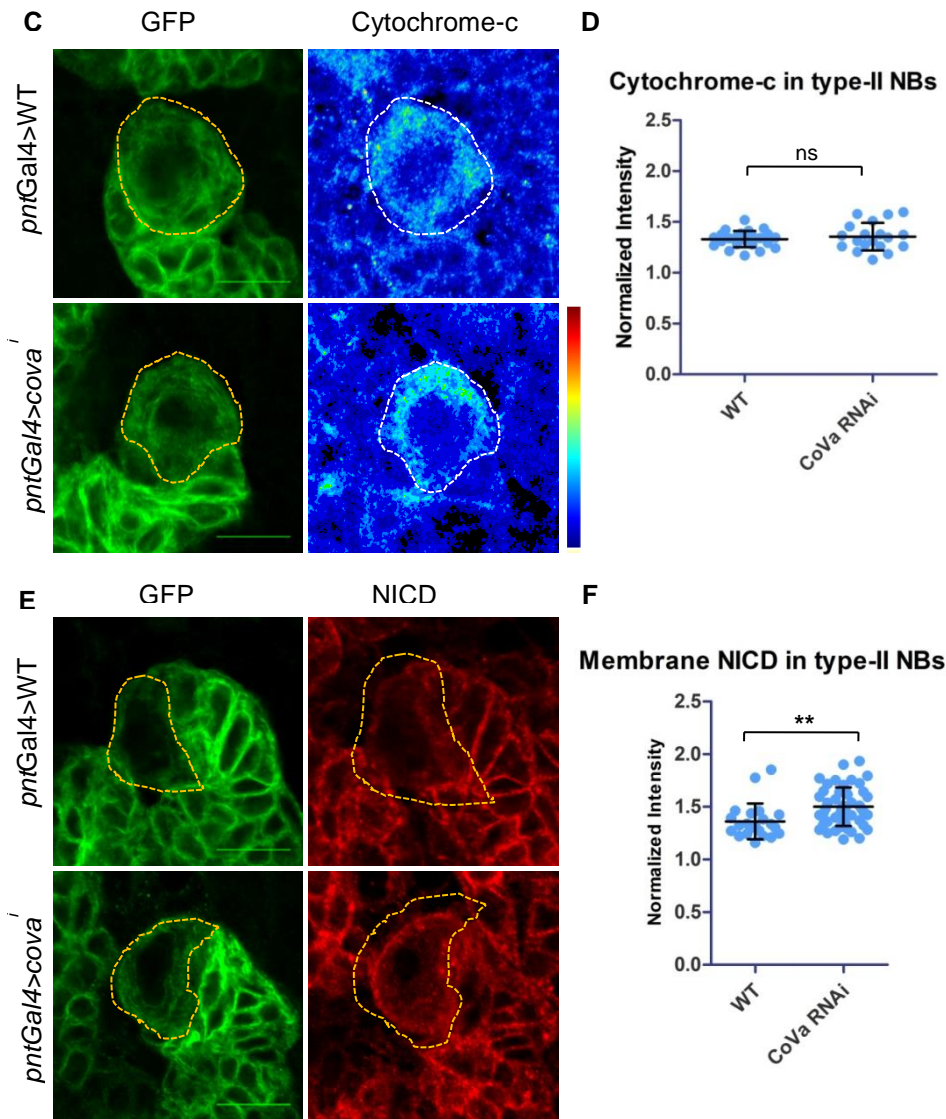


Figure 3.6.2: Inhibition of ETC in type-II neuroblasts decreases ROS and does not affect cytochrome-c in *covai* mutants.

(C) Cytochrome-c expression represented as a heat map in WT, *covai* brains. Dotted lines mark type-II NB cell boundary. (D) Quantification for cytochrome-c fluorescence intensity in (C). $n=(31,18)$ for WT and $(19,6)$ for *covai* (E) Staining of WT and *covai* brains with NICD. (F) Quantification for membrane-enriched localization of NICD in WT and *covai* NBs from (E). $n=(36,16)$ for WT and $(45,10)$ for *covai*. Scale bar = 10 μ m. Analysis was done using an unpaired *t*-test. ns=non-significant, **= $p<0.01$, ***= $p<0.001$.

3.6.2. Mitochondrial morphology is fragmented on pharmacological ETC disruption, but this does not affect NICD distribution

We analyzed mitochondrial morphology upon depletion of cytochrome-c and pharmacological inhibition of ETC with carbonilcyanide p-trifluoromethoxyphenylhydrazine (FCCP). FCCP is a protonophore that disrupts the proton gradient across the inner mitochondrial membrane and uncouples the electron transport chain (Nicholls and Budd, 2000). Notably, mitochondria were fused in the NBs when we downregulated cytochrome-c expression (Fig.3.6.3A) but became fragmented upon FCCP treatment (Fig.3.6.3B). We asked whether the cytoplasmic accumulation of NICD occurred due to mitochondria being depolarized

upon fragmentation in *marf* and *opa1* mutants. To answer this question, we looked at NICD in the NBs in FCCP-treated brains. The NICD signal was not significantly different from the control NBs, indicating that it was not cytoplasmic in the NBs with depolarized mitochondria (Fig.3.6.3C,D), as opposed to that in *opa1* brains (Fig.A2).

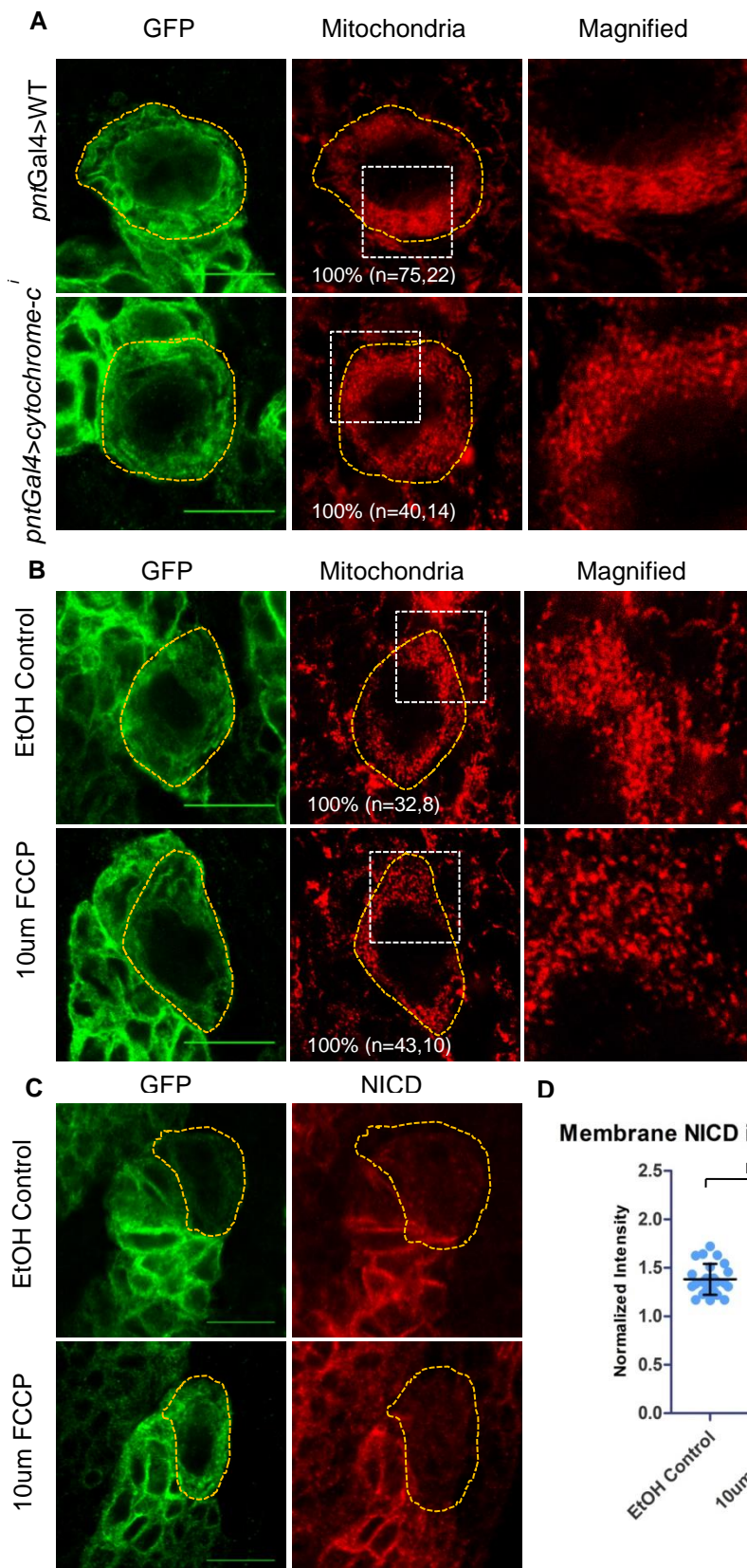


Figure 3.6.3 Analysis of mitochondrial morphology upon inhibition of the ETC.

(A) Super-resolution STED images of mitochondrial morphology type-II NBs upon RNAi-mediated depletion of cytochrome-c. Yellow dotted lines mark NB cell boundary, areas marked by white squares are magnified in the right panels. (B) Super-resolution STED images of mitochondrial morphology type-II NBs upon pharmacological inhibition of the ETC with 10uM FCCP and corresponding EtOH control. Percentages in (A) and (B) indicate frequency of the observed phenotype out of n=(number of NBs, number of brain lobes) type-II NBs recorded. (C) Staining of WT and FCCP-treated brains with NICD. (D) Quantification for membrane-enriched localization of NICD in type-II NBs in control (n=28,10) and FCCP-treated (n=30,8) brains from (C). Scale bar = 10µm. Analysis was done using an unpaired *t*-test. ns=non-significant, **= $p<0.01$, ***= $p<0.001$.

4. Discussion

Our data indicate that mitochondrial fusion is essential for differentiation and lineage progression of type-II neuroblasts in the *Drosophila* larval CNS. Specifically, we have shown that Marf and Opa1 are required for neuroblast differentiation, and loss of these proteins prevents mitochondrial fusion in neuroblasts and decreases the number of differentiated cells present in the NB lineage. Lack of mitochondrial fusion in neuroblasts is accompanied by cytoplasmic accumulation of the cleaved NICD fragment, possibly decreasing signaling activity and reducing the division rate during self-renewal of the NB (Fig. 4.1A). These findings uncover a link between mitochondrial fusion and the Notch pathway in the *Drosophila* CNS. Multiple future directions arise from these data, some of which are discussed below and are currently being pursued.

Cytoplasmic sequestration of NICD and its implications on differentiation

We are currently focussing on determining whether pharmacological inhibition of mitochondrial fusion phenocopies *marf* and *opa1* mutants in terms of cytoplasmic localization of cleaved NICD. One immediate question that follows is whether the inability of NICD to enter the nucleus after perturbing mitochondrial functions stems from either fault in endosomal trafficking or post-translational modifications of the receptor. To illustrate, it is known that E3 ubiquitin ligases can target the Notch receptor to direct its endosomal sorting for either recycling or degradation (Kanwar and Fortini, 2004). Therefore, if inhibition of mitochondrial fusion is upregulating the endocytosis of the Notch receptor, it could impact the steady-state level of the receptor available on the membrane for signaling, thus affecting the activity of the pathway and ultimately NB proliferation rate. We have shown that depletion of Marf and Opa1 in the Notch gain-of-function background alleviates type-II NB hyperproliferation. However it remains to be determined whether this increases differentiation and promotes the formation of GMCs.

NICD is known to accumulate in the cytoplasm when non-canonical signaling is activated (Kasahara and Scorrano, 2014; Perumalsamy et al., 2010), but its implications have not been elucidated. Determining where exactly in the cytoplasm NICD accumulates upon inhibition of mitochondrial fusion would help to answer these questions. It is evident from the cleaved-Notch immunostaining data that the

cytoplasmic signal of cleaved-NICD shows a punctate pattern and is not uniformly distributed throughout the cytoplasm, suggesting that it might be localized on organelles such as mitochondria or autophagosomes. It is hypothesized that NICD prevents mitochondrial fragmentation in the background of Bax-mediated apoptosis when non-canonical signaling is activated, suggesting a direct interaction between NICD and mitochondria. Additionally, analysis of NICD localization in fission-deficient *drp1^{SD}* mutants is required to understand the cause of NICD sequestration to the cytoplasm. For instance, if NICD is nuclear in mitochondrial fission-deficient neuroblasts, then it clearly suggests feedback between mitochondrial morphology and Notch signaling in these cells, with fragmented mitochondria having an impact on the NICD trajectory.

On another note, it has been reported in *Drosophila* neuroblast lineages that the temporal identity of cells affects the expression of Notch target genes (Farnsworth et al., 2015). Neuroblasts and their daughter cells express a series of temporally-regulated transcription factors that correspond with the ‘age’ of the neuroblast leading up to its terminal differentiation. Expression of an ‘old’ transcriptional factor Eyeless/Pax6 in aging cells decreases the ability of these cells to respond to activated Notch signaling. Hence, it would be interesting to look at the temporal transcription factor profile of mitochondrial fusion-deficient neuroblasts. It is possible that early-onset aging decreases the responsiveness of these NBs to Notch signaling and thus decreases NB progeny and lineage size.

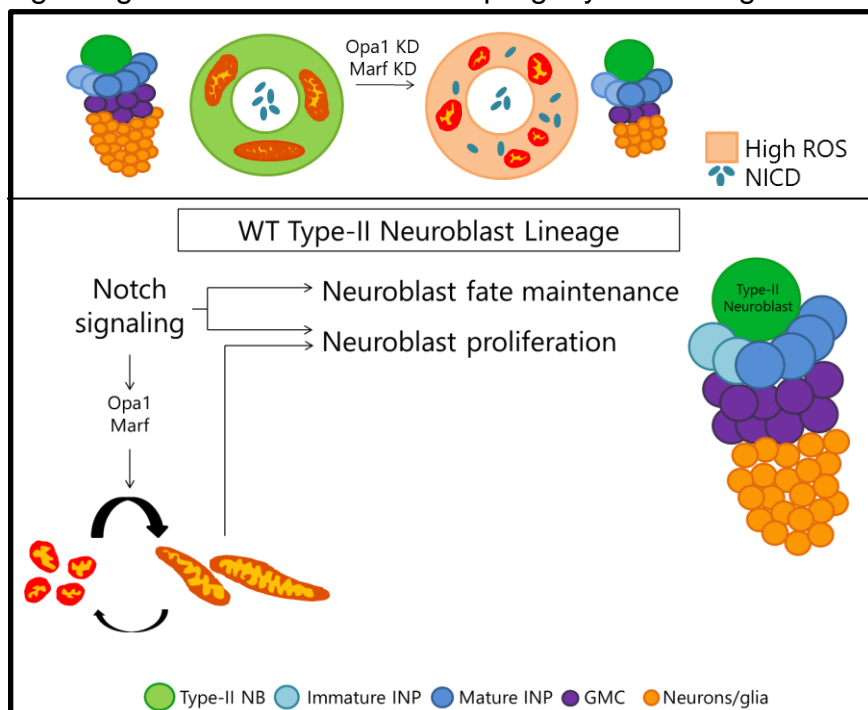


Figure 4.1: Schematic model of the role played by mitochondrial morphology in the differentiation of type-II neuroblasts. (A) Inhibition of mitochondrial fusion decreases differentiation of the type-II NB by sequestering cleaved NICD to the cytoplasm. (B) Proposed feedback between mitochondrial morphology and Notch signaling. Notch signaling promotes mitochondrial fusion in type-II NBs by regulating expression of fusion genes *marf* and *opa1*. Fragmented mitochondria inhibit Notch signaling, thus decreasing NB proliferation and differentiation.

When Notch function is inhibited in type-II neuroblasts using *pntGal4*, we see a decrease in the number of type-II neuroblasts per lobe, mitochondria are less fused in the neuroblasts and proliferation of the neuroblast decreases, resulting in a small lineage with few differentiated cells. In this case, if downregulation of mitochondrial fusion (due to lowered Notch) inhibits neuroblast proliferation, then mitochondrial fragmentation upon *drp1* overexpression should give the same effect and remains to be tested. On the other hand, we know that the proliferation defect due to inhibition of mitochondrial fusion in *opa1* and *marf* mutants is due to perturbation of notch signaling, specifically, cytoplasmic accumulation of NICD. Therefore, it would be interesting to test whether upregulation of *drp1* function also has an effect on notch signaling.

Since expression of *drp1*^{SD} rescues the increase in INP number in *marf* and *opa1* animals, it appears to do so by allowing neuroblast proliferation in a loss of notch background. However, if there is some effect on signaling in the mature INPs in *marf* and *opa1* lineages, this might not be rescued by *drp1*^{SD} expression in the neuroblast, and could be the reason why GMCs are not rescued.

Notch signaling as a regulator of mitochondrial dynamics

Recent evidence in *Drosophila*, as well as mammalian cell types, has uncovered the role of different signaling pathways such as Yorkie, Notch, and EGFR in maintaining mitochondrial morphology (Nagaraj et al., 2012; Perumalsamy et al., 2010; Tomer et al., 2018). Specifically, Notch signaling promotes mitochondrial fusion in mammalian T-cells cells and protects them from Bax-mediated programmed cell death to promote cell survival. As mention previously, a connection between the Notch pathway and mitochondrial function has formerly been reported as a non-canonical signaling axis in *Drosophila* neuroblasts. Notch, together with PTEN-induced kinase 1 (PINK1) regulates mitochondrial respiration and activates Akt signaling to facilitate NB growth and proliferation (Lee et al., 2013). We propose that increase in Notch signaling activity enhances mitochondrial fusion by directly regulating the expression of mitochondrial fusion genes *marf* and *opa1* (Fig. 4.1B). This regulation is perhaps at the transcriptional level, with *marf* and *opa1* being Notch-target genes in *Drosophila* neuroblasts.

Type-II neuroblasts are maintained by transcription factor PointedP1 (*pnt*) when Notch signaling is active (Li et al., 2016). Notch inhibits the expression of *pnt* antagonist Earmuff. Therefore in Notch downregulation mutants, loss of *pnt* expression causes terminal differentiation of type-II neuroblasts. In *opa1* and *marf* mutants, it appears that *pnt* expression is not affected since we always see 8 type-II neuroblasts. This suggests that Notch possibly acts to regulate neuroblast proliferation by maintaining fused mitochondria in type-II neuroblasts in addition to its role in suppressing premature neuroblast differentiation, and this function seems to be specifically affected in *opa1* and *marf* mutants.

Accumulation of ROS can alter differentiation

Reactive oxygen species are known to play a role in cell proliferation, and differentiation in *Drosophila* (Koehler et al., 2017; Owusu-ansah et al., 2008), and an increase in ROS is commonly associated with fragmented mitochondria (Röth et al., 2014). For instance, depletion of Complex-I (*pds* mutant, a subunit of ETC Complex-I) of the electron transport chain is known to cause an increase in ROS levels and a block at the G1-S cell cycle checkpoint. Scavenging ROS in the *pds* background is capable of rescuing the cell cycle defect. Additionally, inhibition of mitophagy in *Drosophila* intestinal stem cells (ISCs) results in early-onset senescence via accumulation of ROS and decreases ISC stemness (Koehler et al., 2017). Therefore, it would be interesting to check if inhibiting ROS accumulation by upregulating enzymes such as superoxide dismutase (SOD) or catalase in the *opa1* background rescues differentiation in the type-II NB lineage.

Cristae remodeling in mitochondria

In a study in the *Drosophila* germline stem cells, it was reported that ATP-synthase is required for stem cell differentiation independent of its role in oxidative phosphorylation (Teixeira et al., 2015). Instead, it is thought to promote cristae maturation in the mitochondria via formation of protein dimers and ETC supercomplexes, which can then regulate differentiation. Therefore, lack of cristae maturation could possibly explain the loss of neuroblast differentiation in mitochondrial fusion-deficient mutants, with the effect being stronger in *opa1* compared to *marf* since Opa1 is known to regulate cristae folding directly (Frezza et al., 2006). Transmission electron microscopy (TEM) analysis of the larval brain in

marf and *opa1* mutants can confirm whether cristae structure is indeed disrupted in fusion-deficient mitochondria, which can then potentially shed light on the role of cristae remodeling in the differentiation of neuroblasts. It would also be interesting to look at the structure of the inner mitochondria membrane in *drp1*^{SD} mutants, and determine whether highly fused mitochondria have serviceable cristae structure.

The effect of calcium homeostasis on signaling pathways

Mitochondrial fusion is essential for proper cardiomyocyte differentiation in the developing mammalian heart (Kasahara et al., 2013). Inhibition of mitochondrial fusion in *Mfn2* and *Opa1* mutants activates Notch signaling via increased Ca²⁺/calcineurin activity, in the end, impairing cardiomyocyte differentiation. Constitutive activation of Ca²⁺-dependent calcineurin function also increases Notch signaling and reduces cardiomyocyte differentiation. This suggests that intracellular calcium homeostasis is crucial for Notch activity irrespective of mitochondrial dynamics and morphology (Kasahara et al., 2013). In *Drosophila*, Marf is known to be associated with the ER-mitochondria contact sites (ERMCS) which are also the site for Ca²⁺ transporters (de Brito and Scorrano, 2008), and depletion of Marf disrupts mitochondrial uptake of calcium. Depletion of *Opa1* is known to enhance mitochondrial Ca²⁺ uptake from the cristae lumen by increasing accessibility of Ca²⁺ to its transporters in the lumen due to compromised cristae integrity (Fulop et al., 2011). Perturbation in Ca²⁺ influx into the mitochondria in neuroblasts affects its lineage progression (Lee et al., 2016); specifically, depletion of mitochondrial fraction of Ca²⁺ reduces NB stemness, whereas increasing mitochondrial uptake of Ca²⁺ induces oxidative stress and programmed cell death. Hence, it needs to be determined whether calcium regulation by mitochondria is disturbed in type-II NBs in mitochondrial fusion-deficient mutants and whether that is the cause of decreased differentiation.

Metabolism and its effect on differentiation

The mitochondrial ETC mutant *cova* seems to behave differently than the mitochondrial morphology mutants. Strikingly, the fact that mitochondria remain fused after depletion of individual components of the ETC and become fragmented only after severe depolarization on FCCP treatment hints at a compensatory mechanism that promotes fusion to minimize stress from defective mitochondria (Jin

and Youle, 2012). Fused mitochondria in *cova* mutants explain stable cytochrome-c level in these NBs compared to fusion-deficient mutants since mitochondrial fusion is typically associated with a higher cristae density and intact cristae structure (Cogliati et al., 2016). Consistent with previous reports, we did not observe an increase in cellular ROS on ComplexIV depletion (Owusu-ansah et al., 2008), but surprisingly, we also did not observe AMPk activation in this mutant. Our data indicate that neuroblasts rely on glycolysis for ATP and not mitochondrial oxidative phosphorylation (Fig.3.4.2 B,F) (Homem et al., 2014), which could explain the lack of AMPk activation in *cova* mutants. Instead, it appears that the loss of differentiation upon depletion of ComplexIV may be related to a slower rate of cell cycle progression as the number of mitotic cells in the lineage decreases. However, the activity of Notch signaling in the *cova* mutant still remains to be tested, particularly the localization of cleaved NICD. Notch analysis can shed light on the mechanism behind the defect in differentiation resulting from downregulation of the electron transport chain. The increase in the membrane fraction of NICD (Fig3.6.2 E,F) suggests that NICD could be enriched on the membrane instead of being in the nucleus in *cova* mutants, resulting in slower proliferation of the neuroblast. Analysis of mitochondrial membrane potential in wild-type neuroblasts as well as the mutants described in this study would be useful to comment on whether perturbation of mitochondrial dynamics and ETC has an effect on the proton gradient across the inner membrane and whether Notch signaling is affected by change in membrane potential as described in previous studies (Tomer et al., 2017).

Altogether, our study adds to the evidence that supports mitochondrial dynamics as an essential factor in cell differentiation apart from its role in mitochondrial energetics. We show that inhibition of mitochondrial fusion can affect signaling in ways different from mitochondrial dysfunction and ROS build-up. Given our findings, the study underscores the interaction between mitochondria and signaling pathways that regulate cell proliferation. In addition to the non-canonical role of Notch in modulating mitochondrial functions, Notch can regulate mitochondrial morphology in neuroblasts, possibly via transcriptional control. In conclusion, we highlight the importance of mitochondrial dynamics in stem cell differentiation in a developmental context.

5. References

- Alexander, C., Votruba, M., Pesch, U.E.A., Thiselton, D.L., Mayer, S., Moore, A., Rodriguez, M., Kellner, U., Leo-Kottler, B., Auburger, G., et al. (2000). OPA1, encoding a dynamin-related GTPase, is mutated in autosomal dominant optic atrophy linked to chromosome 3q28. *Nat. Genet.* 26, 211–215.
- Bello, B.C., Izergina, N., Caussinus, E., and Reichert, H. (2008). Amplification of neural stem cell proliferation by intermediate progenitor cells in *Drosophila* brain development. *Neural Dev.* 3, 5.
- Bigarella, C.L., Liang, R., and Ghaffari, S. (2014). Stem cells and the impact of ROS signaling. *Development* 141, 4206–4218.
- Boone, J.Q., and Doe, C.Q. (2008). Identification of *Drosophila* type II neuroblast lineages containing transit amplifying ganglion mother cells. *Dev. Neurobiol.* 68, 1185–1195.
- Bowman, S.K., Rolland, V., Betschinger, J., Kinsey, K.A., Emery, G., and Knoblich, J.A. (2008). The Tumor Suppressors Brat and Numb Regulate Transit-Amplifying Neuroblast Lineages in *Drosophila*. *Dev. Cell* 14, 535–546.
- Brand, A.H., and Livesey, F.J. (2011). Neural Stem Cell Biology in Vertebrates and Invertebrates: More Alike than Different? *Neuron* 70, 719–729.
- Bray, S. (2006). Notch signalling: a simple pathway becomes complex. *Nat. Rev. Mol. Cell Biol.* 7, 678–689.
- de Brito, O.M., and Scorrano, L. (2008). Mitofusin 2 tethers endoplasmic reticulum to mitochondria. *Nature* 456.
- Chan, D.C. (2006). Mitochondrial Fusion and Fission in Mammals. *Annu. Rev. Cell Dev. Biol.* 22, 79–99.
- Chandel, N.S. (2014). Mitochondria as signaling organelles. *BMC Biol.* 12, 1–7.
- Chen, H., and Chan, D.C. (2005). Emerging functions of mammalian mitochondrial fusion and fission. *Hum. Mol. Genet.* 14, 283–289.
- Chen, H., and Chan, D.C. (2009). Mitochondrial dynamics-fusion, fission, movement, and mitophagy-in neurodegenerative diseases. *Hum. Mol. Genet.* 18, 169–176.
- Cho, J.H., Patel, B., Bonala, S., Manne, S., Zhou, Y., Vadrevu, S.K., Patel, J., Peronaci, M., Ghose, S., Henske, E.P., et al. (2017). Notch transactivates Rheb to maintain the multipotency of TSC-null cells. *Nat. Commun.* 8.
- Cogliati, S., Frezza, C., Soriano, M.E., Varanita, T., Quintana-Cabrera, R., Corrado, M., Cipolat, S., Costa, V., Casarin, A., Gomes, L.C., et al. (2013). Mitochondrial cristae shape determines respiratory chain supercomplexes assembly and respiratory efficiency. *Cell* 155, 160–171.
- Cogliati, S., Enriquez, J.A., and Scorrano, L. (2016). Mitochondrial Cristae : Where Beauty Meets Functionality. *Trends Biochem. Sci.* 41, 261–273.
- Farnsworth, D.R., Bayraktar, O.A., and Doe, C.Q. (2015). Aging neural progenitors lose competence to respond to mitogenic Notch signaling. *Curr. Biol.* 25, 3058–3068.
- Frezza, C., Cipolat, S., Martins de Brito, O., Micaroni, M., Beznoussenko, G. V., Rudka, T., Bartoli, D., Polishuck, R.S., Danial, N.N., De Strooper, B., et al. (2006). OPA1 Controls Apoptotic Cristae Remodeling Independently from Mitochondrial Fusion. *Cell* 126, 177–189.
- Fulop, L., Szanda, G., Enyedi, B., Varnai, P., and Spat, A. (2011). The Effect of OPA1 on Mitochondrial Ca²⁺ Signaling. *PLoS One* 6, 31–34.
- Hans, F., and Dimitrov, S. (2001). Histone H3 phosphorylation and cell division. *Oncogene* 20, 3021–

3027.

Hardie, D.G., Ross, F.A., and Hawley, S.A. (2012). AMPK: A nutrient and energy sensor that maintains energy homeostasis. *Nat. Rev. Mol. Cell Biol.* *13*, 251–262.

Homem, C.C.F., and Knoblich, J.A. (2012). *Drosophila* neuroblasts: a model for stem cell biology. *Development* *139*, 4297–4310.

Homem, C.C.F., Steinmann, V., Burkard, T.R., Jais, A., Esterbauer, H., and Knoblich, J.A. (2014). Ecdysone and Mediator Change Energy Metabolism to Terminate Proliferation in *Drosophila* Neural Stem Cells. *Cell* *158*, 874–888.

Jin, S.M., and Youle, R.J. (2012). PINK1- and Parkin-mediated mitophagy at a glance. *J. Cell Sci.* *125*, 795–799.

Kanwar, R., and Fortini, M.E. (2004). Notch signaling: A different sort makes the cut. *Curr. Biol.* *14*, 1043–1045.

Kasahara, A., and Scorrano, L. (2014). Mitochondria: From cell death executioners to regulators of cell differentiation. *Trends Cell Biol.* *24*, 761–770.

Kasahara, A., Cipolat, S., Chen, Y., Dorn, G.W., and Scorrano, L. (2013). Mitochondrial Fusion Directs Cardiomyocyte Differentiation via Calcineurin and Notch Signaling. *Science* (80-.). *342*, 734–737.

Khacho, M., Clark, A., Svoboda, D.S., Azzi, J., MacLaurin, J.G., Meghaizel, C., Sesaki, H., Lagace, D.C., Germain, M., Harper, M.E., et al. (2016). Mitochondrial Dynamics Impacts Stem Cell Identity and Fate Decisions by Regulating a Nuclear Transcriptional Program. *Cell Stem Cell* *19*, 232–247.

Koehler, C.L., Perkins, G.A., Ellisman, M.H., and Jones, D.L. (2017). Pink1 and Parkin regulate *Drosophila* intestinal stem cell proliferation during stress and aging. *J. Cell Biol.* *216*, 2315–2327.

Lee, K.S., Wu, Z., Song, Y., Mitra, S.S., Feroze, A.H., Cheshier, S.H., and Lu, B. (2013). Roles of PINK1, mTORC2, and mitochondria in preserving brain tumor-forming stem cells in a noncanonical Notch signaling pathway. *Genes Dev.* *27*, 2642–2647.

Lee, S., Lee, K.S., Huh, S., Liu, S., Lee, D.Y., Hong, S.H., Yu, K., and Lu, B. (2016). Polo Kinase Phosphorylates Miro to Control ER-Mitochondria Contact Sites and Mitochondrial Ca²⁺ Homeostasis in Neural Stem Cell Development. *Dev. Cell* *37*, 174–189.

Li, X., Xie, Y., and Zhu, S. (2016). Notch maintains *Drosophila* type II neuroblasts by suppressing the expression of the Fez transcription factor Earmuff. *Development* *143*, 2511–2521.

Mcbride, H.M., and Neuspiel, M. (2006). Mitochondria : More Than Just a Powerhouse. *Curr. Biol.* *551*–560.

Mishra, P., and Chan, D.C. (2014). Mitochondrial dynamics and inheritance during cell division, development and disease. *Nat. Rev. Mol. Cell Biol.* *15*, 634–646.

Mishra, P., and Chan, D.C. (2016). Metabolic regulation of mitochondrial dynamics. *J. Cell Biol.* *212*, 379–387.

Mitra, K., Rikhy, R., Lilly, M., and Lippincott-Schwartz, J. DRP1-dependent mitochondrial fission initiates follicle cell differentiation during. *197*, 487–497.

Nagaraj, R., Gururaja-rao, S., Jones, K.T., Slattery, M., Negre, N., Braas, D., Christofk, H., White, K.P., Mann, R., and Banerjee, U. (2012). Control of mitochondrial structure and function by the Yorkie / YAP oncogenic pathway. *Genes Dev.* *26*, 2027–2037.

Nicholls, D.G., and Budd, S.L. (2000). Mitochondria and Neuronal Survival. *Physiol. Rev.* *80*, 315–360.

Noguchi, M., and Kasahara, A. (2017). Mitochondrial dynamics coordinate cell differentiation.

Biochem. Biophys. Res. Commun. 1–6.

Owusu-ansah, E., Yavari, A., Mandal, S., and Banerjee, U. (2008). Distinct mitochondrial retrograde signals control the G1-S cell cycle checkpoint. *Nat. Genet.* *40*, 356–361.

Paull, T.T., Rogakou, E.P., Yamazaki, V., Kirchgessner, C.U., Gellert, M., and Bonner, W.M. (2000). A critical role for histone H2AX in recruitment of repair factors to nuclear foci after DNA damage. *Curr. Biol.* *10*, 886–895.

Perumalsamy, L.R., Nagala, M., and Sarin, A. (2010). Notch-activated signaling cascade interacts with mitochondrial remodeling proteins to regulate cell survival. *Proc. Natl. Acad. Sci. U. S. A.* *107*, 6882–6887.

Röth, D., Krammer, P.H., and Gülow, K. (2014). Dynamin related protein 1-dependent mitochondrial fission regulates oxidative signalling in T cells. *FEBS Lett.* *588*, 1749–1754.

Scorrano, L. (2009). Opening the doors to cytochrome c: Changes in mitochondrial shape and apoptosis. *Int. J. Biochem. Cell Biol.* *41*, 1875–1883.

Teixeira, F.K., Sanchez, C.G., Hurd, T.R., Seifert, J.R.K., Czech, B., Preall, J.B., Hannon, G.J., and Lehmann, R. (2015). ATP synthase promotes germ cell differentiation independent of oxidative phosphorylation. *Nature* *17*, 689–695.

Tomer, D., Chippalkatti, R., Mitra, K., and Rikhy, R. (2018). ERK regulates mitochondrial membrane potential in fission deficient *Drosophila* follicle cells during differentiation. *Dev. Biol.* *434*, 48–62.

Wallace, D.C., Fan, W., and Procaccio, V. (2011). Mitochondrial Energetics and Therapeutics. *Annu. Rev. Pathol.* *5*, 297–348.

Wang, H., Somers, G.W., Bashirullah, A., Heberlein, U., Yu, F., and Chia, W. (2006). Aurora-A acts as a tumor suppressor and regulates self-renewal of *Drosophila* neuroblasts. 3453–3463.

Zacharioudaki, E., Magadi, S.S., Delidakis, C., Alifragis, P., Poortinga, G., Parkhurst, S.M., Delidakis, C., Almeida, M.S., Bray, S.J., Babaoglan, A.B., et al. (2012). bHLH-O proteins are crucial for *Drosophila* neuroblast self-renewal and mediate Notch-induced overproliferation. *Development* *139*, 1258–1269.

Züchner, S., Mersiyanova, I. V., Muglia, M., Bissar-Tadmouri, N., Rochelle, J., Dadali, E.L., Zappia, M., Nelis, E., Patitucci, A., Senderek, J., et al. (2004). Mutations in the mitochondrial GTPase mitofusin 2 cause Charcot-Marie-Tooth neuropathy type 2A. *Nat. Genet.* *36*, 449–451.

6. Appendix

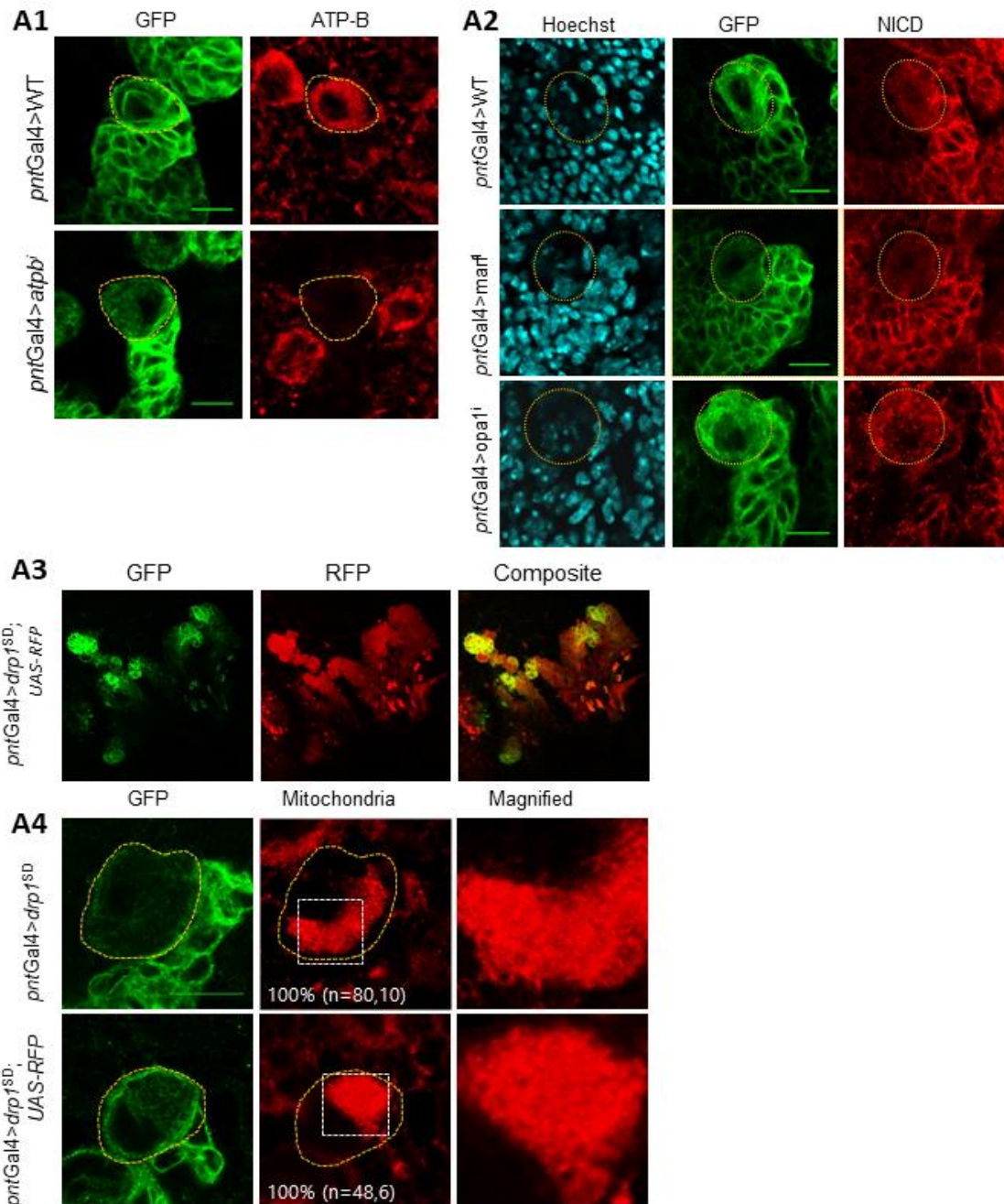


Figure A1: Staining of WT and *atpb¹* brains with anti-ATP β antibody. Yellow dotted lines mark type-II NB cell boundary. n= (11,4) for WT and (11,4) for *atpb¹*. Scale bar = 10 μ m.

Figure A2: Staining of WT, *marf* and *opa1¹* brains with anti-NICD antibody. Yellow dotted lines mark type-II NBs. n= (24,10) for WT, (19,12) for *marf* and (26,12) for *opa1¹*. Scale bar = 10 μ m.

Figure A3 and A4: Gal4-dilution control for *drp1^{SD}* mutants. (A3) RFP expression in type-II NB lineages. (A4) Super-resolution STED images for mitochondrial morphology in *drp1^{SD}* alone and *drp1^{SD}; UAS-RFP*. Percentage indicates frequency of observed phenotype in n=(number of type-II NBs, number of lobes) recorded. Yellow dotted line marks NB cell boundary, areas marked by white squares are magnified in the right panels. Scale bar = 10 μ m.